ORIGINAL ARTICLE

Experimental analysis of allergenic tree pollen deposition in a three-dimensional anatomical model of the adult nasal cavity

Anna Rapiejko[1ABCDEFG], Tomasz R. Sosnowski[2ABCDEF], Krzysztof Sosnowski[3AEF], Dariusz Jurkiewicz[1ADF]

[1]Department of Otolaryngology and Laryngological Oncology with Clinical Department of Cranio-Maxillofacial Surgery, Military Institute of Medicine – National Research Institute, Warsaw, Poland
[2]Faculty of Chemical and Process Engineering, Warsaw University of Technology, Warsaw, Poland
[3]Institute of Control and Industrial Electronics, Faculty of Electrical Engineering, Warsaw University of Technology, Warsaw, Poland

ABSTRACT:

Introduction: Exposure to pollen allergens is one of the key environmental factors determining the occurrence of allergic rhinitis. In Central Europe, tree pollen plays a significant role in triggering symptoms of inhalant allergy in the spring months.

Aim: This study evaluated the deposition of tree pollen grains in a 3D anatomical model of the adult nasal cavity under varying flow rates (5 L/min, 7.5 L/min, and 20 L/min per nostril).

Material and methods: Original methods of analysis were developed, including macroscopic analysis of photographs reflecting tree pollen deposits on the surface of the lateral wall of a printed 3D anatomical model of the nasal cavity and nasal septum, and microscopic evaluation of pollen collected from selected parts of the nasal geometry. The macroscopic analysis was supplemented with original software for the quantitative determination of areas covered with pollen deposits.

Results: The results showed statistically significant differences in the regional deposition of pollen grains of different sizes in the nasal cavity, depending on the flow conditions. The deposition of birch, alder, and hazel pollen grains in the nasal cavity exhibits similar characteristics, with significant differences between the individual segments of the lateral wall and the nasal septum. While the middle segment of the lateral wall accounted for the largest segment share of the total lateral wall deposition, the highest relative pollen deposition in relation to the segment area was found in the front segment. The posterior segment of the lateral wall showed a marginal contribution to the deposition process. The most significant percentage of the segment area of the nasal septum covered with pollen was recorded in the anterior segment. However, the posterior segment accounted for a larger share of the total septal deposition due to its larger surface area. Consistent findings describe deposits of large pollen grains from pine and spruce trees. The values of segmental pollen deposition in the anterior segment were significantly higher than in the other segments. The deposition on the nasal septum was significantly greater in the anterior than in the posterior segment. Lateral wall share % and septal share % tended to increase with increasing airflow through the nasal cavity, reaching their highest values at 20 L/min. The intensification of airflow led to a shift in the location of maximum pollen deposition towards the anterior sections of the nose, with a simultaneous reduction in pollen penetration into the posterior segments.

Conclusions: The study confirms the role of inertial effects in the flow and deposition of aerosols in the nasal cavity, indicating that the large size of pollen grains and higher airflow rates promote pollen deposition mainly in the anterior regions of the lateral wall and nasal septum. However, it also shows that other deposition mechanisms, such as direct interception in the case of grain aggregates, and differences in effective particle density, may influence the spatial distribution of deposited pollen in the nasal cavity. The results obtained should facilitate the control of allergen exposure and the use of topical treatment.

KEYWORDS: 3D model of nasal cavity, nasal deposition, tree pollen

Received: 07.07.2025
Accepted: 29.08.2025
Published: 15.09.2025

CITE THIS ARTICLE AS:
Rapiejko A., Sosnowski T.R., Sosnowski K., Jurkiewicz D.: Experimental analysis of allergenic tree pollen deposition in a three--dimensional anatomical model of the adult nasal cavity; Otolaryngol Pol 2025; 79 (5): 25–44; DOI: 10.5604/01.3001.0055.2572

AUTHORS' CONTRIBUTION:
A. Conceptualization
B. Data Curation
C. Formal Analysis
D. Funding Acquisition
E. Investigation
F. Methodology
G. Project Administration

CORRESPONDING AUTHOR:
Anna Rapiejko MD (ORCID: 0000--0002-8906-2405); Department of Otolaryngology and Laryngological Oncology with Clinical Department of Cranio-Maxillofacial Surgery, Military Institute of Medicine – National Research Institute; Szaserow street 128, 04-141 Warsaw, Poland;
Phone: +48 728188744;
E-mail: anna.rapiejko@obas.pl

COPYRIGHT:
Some rights reserved: Polish Society of Otorhinolaryngologists Head and Neck Surgeons. Published by Index Copernicus Sp. z o.o.

OPEN ACCESS:
The content of the journal „Polish Society of Otorhinolaryngologists Head and Neck Surgeons" is circulated on the basis of the Open Access which means free and limitless access to scientific data.

CREATIVE COMMONS CC BY:
This material is available under the Creative Commons – Attribution NonCommercial 4.0 International (CC BY-NC 4.0). The full terms of this license are available on: https://creativecommons.org/licenses/by-nc/4.0/Legalcode

COMPETING INTERESTS:
The authors declare that they have no competing interests.

ABBREVIATIONS

3D – three–dimensional
AMNC – anatomical model of nasal cavity
ANOVA – analysis of variance
CFD – computational fluid dynamics
FBD – fluidised bed dispenser
IQR – interquartile range
NADPH – nicotinamide adenine dinucleotide phosphate
PSD – particle size distribution
SA – septum anterior
SEM – scanning electron microscopy
SP – septum posterior
STL – stereolithography
WA – wall anterior
WM – wall middle
WP – wall posterior

INTRODUCTION

The biosphere is the source of primary biogenic aerosol particles. Among the many components of natural bioaerosols are pollen grains, which are the male gametes of wind-pollinated (anemophilous) seed plants. They are typically small in size (ranging from 15 to 90 μm), very light in mass, aerodynamic, and produced in large quantities. Once airborne during the pollen season, they are carried by the wind over various distances [1].

The nose is the entry site for the majority of inspired air, which is humidified and filtered on its way to the lower airways. Pollen grains, being the component of inspired air, enter the nasal cavity, where they undergo filtration [2]. The importance of particular pollen in inducing allergic reactions in the nasal mucosa depends on their abundance in the atmosphere and the pollen allergenic potency [3].

In Central Europe, the pollen of trees belonging to the *Fagales* order, the *Betulaceae* family, represented by birch (*Betula*), alder (*Alnus*), and hazel (*Corylus*), play a significant role in causing allergy symptoms during the spring months, with birch being the main culprit. Periods of intense pollen release from hazel and alder precede the birch pollen season, which may be responsible for the phenomenon known as "priming effect" of the mucous membrane, which prepares it for contact with birch allergens [4–6]. Through the "priming effect", early exposure lowers the sensitivity threshold for triggering symptoms later in the pollen season [7, 8]. The role of the "priming effect" in grass pollen allergies is attributed to prior exposure to conifer pollen; pine (*Pinus*), and spruce (*Picea*), which are present in large quantities in the air in the period preceding the grass pollen season. However, they are not generally considered allergenic themselves.

Exposure to pollen allergens represents a key factor among environmental determinants of allergic rhinitis. When pollen grains come into contact with the nasal mucosa, they are moistened by small apertures, which leads to their activation and the release of allergenic proteins, triggering an IgE-mediated cascade of allergic reaction and causing symptoms such as rhinorrhea, nasal obstruction, nasal itching, and sneezing [9]. The most dominant allergen of *Fagales* trees, to which 95% of birch-sensitive individuals react, is Bet v 1, the major birch pollen allergen, belonging to the PR-10 protein family [10]. The main allergens of other members of the *Fagales* order, which are homologues of Bet v 1, also belong to this family of proteins; Aln g 1 for alder, Cor a 1 for hazel. Some other allergens have been described in pollen grains of the *Fagales*, representing, among others, the profilin, polcalcin, and cyclophilin families. There is a high level of allergenic cross-reactivity between the representative plants of the genera belonging to the order *Fagales* [11]. Pollen grains also release non-allergenic products: lipids, adenosine, NADPH oxidases, and proteases, which can enhance the immune response [10, 12].

The main factors affecting particle deposition in the nasal cavity are the flow rate of inhaled air, particle characteristics, and the geometry of the nasal airways. There are various mathematical and statistical models for calculating the deposition of particles within the human nose [13]. However, to the best of our knowledge, there are few studies available on the deposition of pollen grains in nasal cavities, most of which rely on CFD, a new tool in rhinology that uses engineering techniques to model nasal airflow mathematically [14–17].

The development of 3D printing techniques has made it possible to produce highly accurate physical models of anatomical structures used for *in vitro* studies. However, there have been very few attempts to map real-world conditions of deposition of pollen grains on a 3D printed model of the nasal cavity [16, 18], which provide realistic images regarding particle-deposition patterns. Experimental work plays an important role in the validation of CFD models [13].

Interdisciplinary research, combining knowledge of allergology and aerobiology with the ability to measure and analyse the dynamics of dispersed systems, can make a valuable contribution to the field. The research will help determine the influence of pollen type, characterised by shape and size (dependent on plant species) and breathing pattern (dependent on activity, among other factors), on the site of pollen grain deposition in the nasal cavity. Understanding how pollen is deposited in the nasal airways may prove useful in preventing and treating nasal allergic diseases.

AIM

The study aimed to experimentally analyse the nasal deposition of allergenic tree pollen in a three-dimensional anatomical model of the adult nasal cavity at various constant flow rates.

MATERIAL AND METHODS

Pollen-handling protocol

The pollen season is assessed based on monitoring carried out in accordance with the recommendations of the European Aeroallergen Network, using the continuous volumetric method [19]. The characteristics of the pollen season are described by many variables, including the start of the pollen season, which is forecast annually based on extensive data [20].

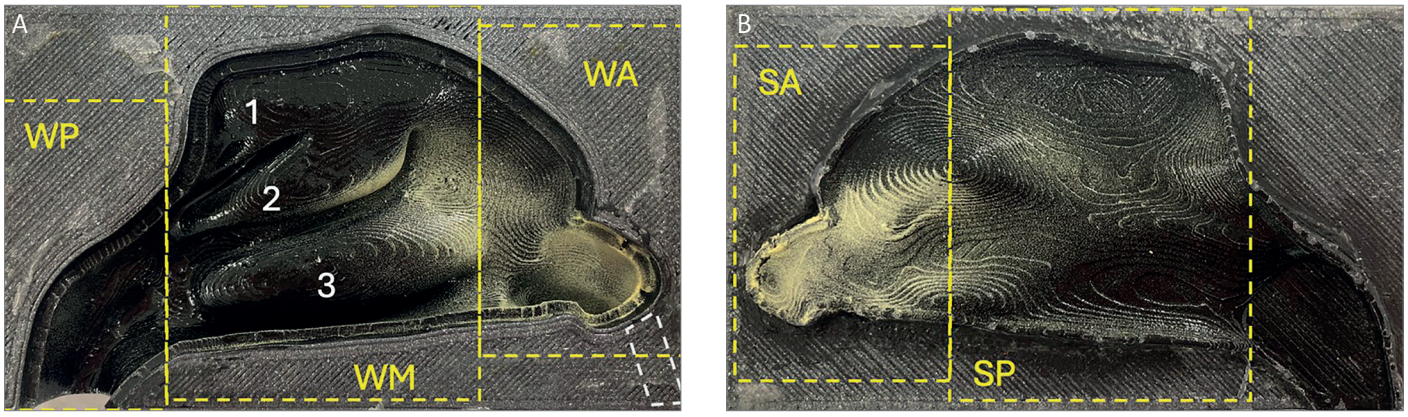

Fig. 1. Two sides of 3D printouts of the nasal surface: (A) lateral wall with the nasal concha (1–3), (B) septum. Yellow contours show the segments used in the deposition analysis WA – wall anterior, WM – wall middle, WP – wall posterior, SA – septum anterior, SP – septum posterior. The white dotted line indicates the location of the air inlet (corresponding to the nostril, not visible on the photograph).

In Poland, representatives of the *Corylus, Alnus*, and *Betula* genera are the main sources of pollen allergens in the air in the early spring months [4–6]. The pollen season for hazel (*Corylus*), a monoecious shrub characterised by drooping yellow male catkins and small female inflorescences, typically begins in February. Under favourable weather conditions, hazel pollen grains may appear in the air at the turn of January and February. Pollination of alder (*Alnus*), a monoecious tree with flowers arranged in unisexual inflorescences, begins in February. The flowers of the birch tree (*Betula*), characterised by a white trunk, drooping branches, and hanging yellow-green catkins, open at the turn of March and April. In April, the air is filled with highly allergenic birch pollen. Pine (*Pinus)* and spruce (*Picea)*, common conifers in Poland, release pollen in May.

These tree species are not protected in Poland, so collecting material for research did not require any specific permission and was performed on public land. Data on pollen counts in Warsaw were obtained from monitoring conducted by the Allergen Research Center. Phenological observations of specimens helped determine the appropriate time for inflorescence collection. Approximately 100 catkins were collected from each specimen before the flowers were fully open, and then stored in a dry place for several days [21]. Ripe pollen grains released from microsporangia were sieved by special sieves when signs of pollen shedding in catkins were recorded. Since dry pollen remains viable at room temperature with low relative humidity for several days, the experiments were conducted within this time frame [22]. Pollen grains from five different species were used in the study: *Corylus avellana, Alnus glutinosa, Betula pendula, Pinus sylvestris,* and *Picea abies*.

Pollen characterization

Three techniques were used to characterise pollen grains: scanning electron microscopy (model TM-1000, Hitachi, Japan) at 250–4000x magnification, light microscopy at 400x magnification, and PSD measurement in the aerosol phase using laser diffraction (Spraytec, Malvern Instruments, UK). Details of light microscopy examinations are presented below. Pollen aerosols for laser diffraction studies were generated in the fluidised bed dispenser described in the section below.

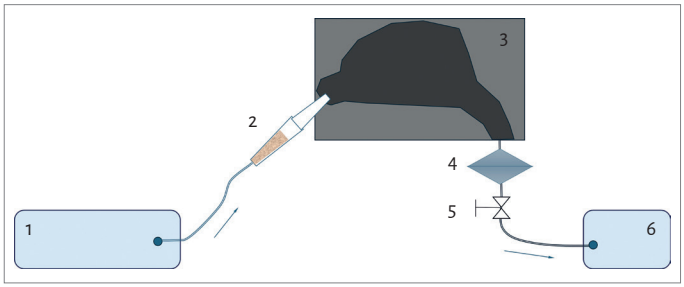

Fig. 2. Schematic diagram of the experimental system: 1 – compressor, 2 – fluidised bed dispenser (FBD), 3 – anatomical model of the nasal cavity (AMNC), 4 – filter, 5 – valve with flowmeter, 6 – vacuum pump. The arrows indicate the airflow direction.

Anatomical 3D model of the nasal cavity

The methodology of the experiments was initially described and validated by Sosnowski et al. [23]. The study was conducted using an anatomical model of the nasal cavity. Nasal geometry was adapted from the data by Bruning et al. [24]. One part of the nasal cavity was included, justified by the results of previous studies on the deposition of intranasal corticosteroids, which demonstrated the usefulness of this approach for analysing regional deposition on both the lateral wall of the nose and the nasal septum [25, 26]. STL files of the nasal geometry were developed using open-source software (Blender version 4.1.10) to prepare models of the two parts, allowing easy assembly for further deposition experiments. The model was printed on an Ender 3 printer (Creality, Shenzen, China) using a grey-black PLA filament (210°C printing temperature, 0.3 mm layer height, 0.8 mm nozzle width). The inner surfaces of the 3D AMNC prints were painted black to improve the contrast of the yellowish pollen grain deposits. The printouts are shown in Fig. 1. The nose division used was based on earlier models, which showed significant variability in airflow characteristics and particle deposition in these areas [27]. Before deposition tests, these surfaces were coated with a thin layer of a viscous solution (1% Triton X-100 in glycerol) to mimic nasal mucus and prevent the reflection or re-emission of pollen grains.

Deposition analysis with macroscopic image analysis

Aerosolisation of pollen, both in the PSD analysis and during nasal deposition measurements, was performed using air supplied from

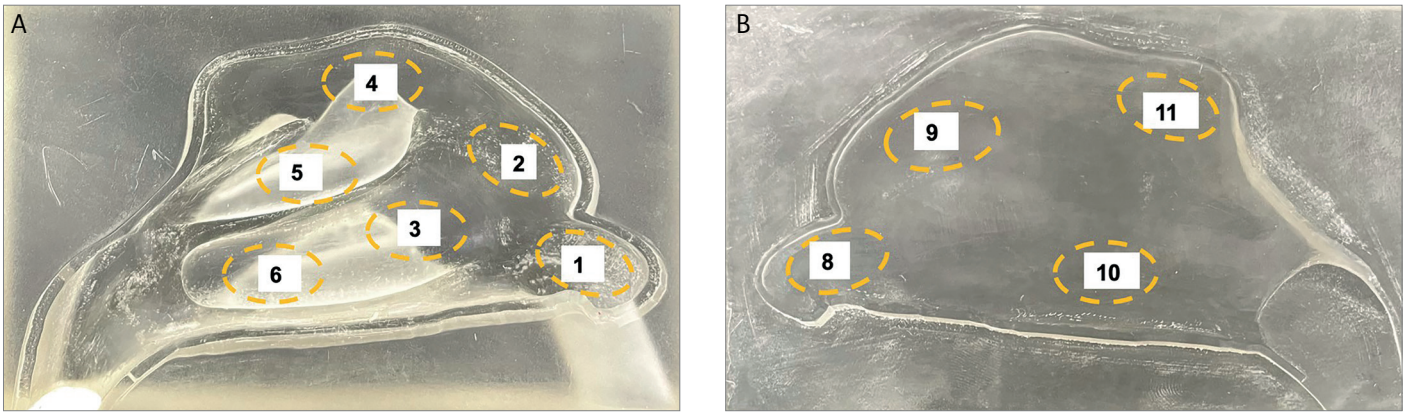

Fig. 3. Location of the analysed stripes (A) on the nasal lateral wall (B) on the nasal septum.

the compressor of the medical nebuliser (model Nano, Diagnostics, Poland) to a made-in-house fluidised bed dispenser. The schematic diagram of the experimental system is shown in Fig. 2.

Approximately 50 mg (±10%) of pollen was loaded into the dispenser. The dose of aerosol emitted was measured using an analytical balance (Radwag, Poland). The aerosolised pollen was evacuated from FBD by switching on the compressor for 5–10 seconds. Airflow through the AMNC was generated using a laboratory vacuum pump and adjusted by a valve to desired values, reflecting different levels of body activity as indicated by the mass flow meter (model 4040, TSI Inc., USA). Experiments were conducted in a unilateral (single-cavity) configuration, with inlet flow rates of 5, 7.5, and 20 L/min applied per nostril (approximately 10, 15, and 40 L/min bilaterally, assuming an ideal 50/50 split although in reality, this split varies depending on the nasal cycle and left-right resistance asymmetry).

During deposition experiments, the 3D AMNC was clamped between rigid plastic plates with the appropriate positioning marked to ensure repeatability of measurements and to distribute the pressure evenly across the model. Nasal cavity deposition measurements were performed after inserting the emitter tip of the dispenser into the nostril when air flow through the AMNC was activated. The dispenser was aligned with the nostril's central axis to maximise delivery efficiency. After depositing the aerosol in the AMNC and turning off the compressor and the vacuum pump, the model was dismantled. Each part (lateral wall of the nasal cavity and septum) was photographed using an iPhone X (Apple, Cupertino, USA), and the photos were analysed using an originally developed software written in Python [23]. The software enabled the identification and analysis of areas of the nasal surface covered with deposits in the segments of each side of the AMNC geometry (Fig. 1).

Deposition analysis with microscopic evaluation of slides

An additional method of assessing nasal pollen deposition was done by applying strips of tape coated with a silicone solution (Lanzoni, Bologna, Italy) on the AMNC surface. Their location on the nasal cavity model is shown in Fig. 3.

Strips (1.3 cm x 1 cm) were attached to the lateral wall of the nasal cavity model in six selected locations: 1. in the nasal vestibule, anterior-inferior part, in front of the beginning of the inferior nasal concha, 2. in the anterior part of the nasal cavity, above the nasal vestibule, in front of the middle nasal concha, 3. in the middle part of the inferior nasal concha, 4. the upper-anterior part of the middle nasal concha, near the transition to the superior nasal meatus, 5. in the middle part of the middle nasal concha, and 6. in the posterior part of the inferior nasal concha.

Four locations for the strips were marked on the model of the nasal septum: 8. in the anterior-inferior part of the cartilaginous septum, close to the mobile part of the septum, 9. in the upper front part of the cartilaginous septum, below the roof of the nose 10. in the lower posterior part of the septum, along the vomer bone, 11. in the upper posterior part of the septum.

The method of pollen aerosol application to the nasal cavity model was the same as described in the section above. After the deposition experiment and dismantling of the model, the strips were used as substrates for microscopic slides. The slides, mounted in glycerine jelly with fuchsine (Lanzoni, Bologna, Italy), were analysed under a light microscope at 400x magnification. Light microscopy is one of the most effective methods for the qualitative and quantitative analysis of pollen grains, which exhibit unique morphological characteristics based on their shape, size, and other morphological features. Pollen grains that cannot be identified due to degradation or damage are recorded as "Undetermined" or "Damaged" [11, 28]. The analysis covers not only the number of pollen grains deposited in specific areas of the nasal cavity, but also their condition/appearance, which can be used to assess how the structure and possible fragmentation of pollen grains are related to the site of deposition in the nasal cavity.

Statistical analysis

Two outcome variables, expressed as percentages, were analysed: (1) segmental surface deposition (referred to as segmental deposition) defined as the percentage of the given segment's surface area covered by pollen; and (2) the segment share of total lateral wall deposition/segment share of total septal deposition (referred to as lateral wall share % / septal share %), defined as the percentage of the entire lateral wall (or septum) covered by pollen assigned to a given segment (area-weighted). The measurements for the segments were paired (same objects): lateral wall – segments WA/WM/WP; septum – SA/SP. The tests were conducted under three steady flow rates

(5 L/min, 7.5 L/min, 20 L/min per nostril) for 5 types of aerosol. For each combination (aerosol × flow rate × wall), the 'segment' effect was verified by one-way analysis of variance (ANOVA). Due to small sample sizes and possible violations of assumptions, a non-parametric test was used in parallel: Kruskal-Wallis (comparisons between groups). The planned pair contrasts (WA–WM, WA–WP; in the SA–SP septum) were assessed using the paired samples t-tests. Combined analyses were also performed after merging the flows within each aerosol and after merging all aerosols, using a similar test scheme. The report included F statistics, degrees of freedom, p-values and effect size (η^2); all tests were two-tailed at $\alpha = 0.05$, and the Holm–Bonferroni correction was used for multiple comparisons. It was assumed, according to Cohen, that $\eta^2 > 0.14$ indicates a large effect size. The distributions were presented, among others, in box plots. Descriptive statistics were used to analyse data from microscopic slides.

RESULTS

Characterization of pollen size and morphology

Fig. 4. presents SEM images of pollen grains, demonstrating that the size and morphology of the grains are consistent with the known description; pine and spruce pollen grains have a different morphology than hazel pollen grains and are noticeably larger. The average maximum size was as follows: hazel pollen ~20–30 µm, pine pollen ~50 µm, and spruce pollen ~70 µm. It must be noted, however, that SEM images are done in a vacuum, which can influence the original grain morphology and size. Therefore, the images obtained with light microscopy, shown in Fig. 5.–6., bring additional, more realistic data.

Hazel (*Corylus)* pollen grains are suboblate or subtriangular, usually 22–30 µm in size, triporate with large onci (lens-shaped structures that occur below the apertures) (Fig. 5A.). Alder (*Alnus)* pollen grains are subolate, 20–35 µm in size, with five pores around the equator, with small clear onci (Fig. 5B.). Birch (*Betula*) pollen grains, most often measuring 18-30 µm in size, are suboblate to spheroidal, triporate with small onci [29] (Fig. 5C.).

A different pollen morphology characterises coniferous trees. Pine (*Pinus*) pollen grains are quite big (50–60 µm in size) and have two air-filled sacs with a single long furrow between them (Fig. 6A.). Thick and rough exine is on the dorsal surface. Thanks to the presence of sacs, *Pinus* pollen grains are very buoyant. Spruce *(Picea)* pollen grains are slightly larger (50–90 µm in size), but very similar in morphology to *Pinus* pollen. However, the sacs are small in proportion to the size of the grain, and the furrow forms a shallow groove between the sacs (Fig. 6B.) [29, 30].

Laser diffraction analysis of pollen aerosols of birch, alder, hazel, pine, and spruce, after release from the FBD, revealed distinct differences in size distribution profiles (Fig. 7.). Birch pollen showed the broadest and most polydisperse distribution, with two clear modes: a dominant one at 15–30 µm and a secondary at 100–200 µm, indicating both single grains and agglomerates. Alder pollen exhibited a bimodal profile, dominated by particles in the 18–35 µm

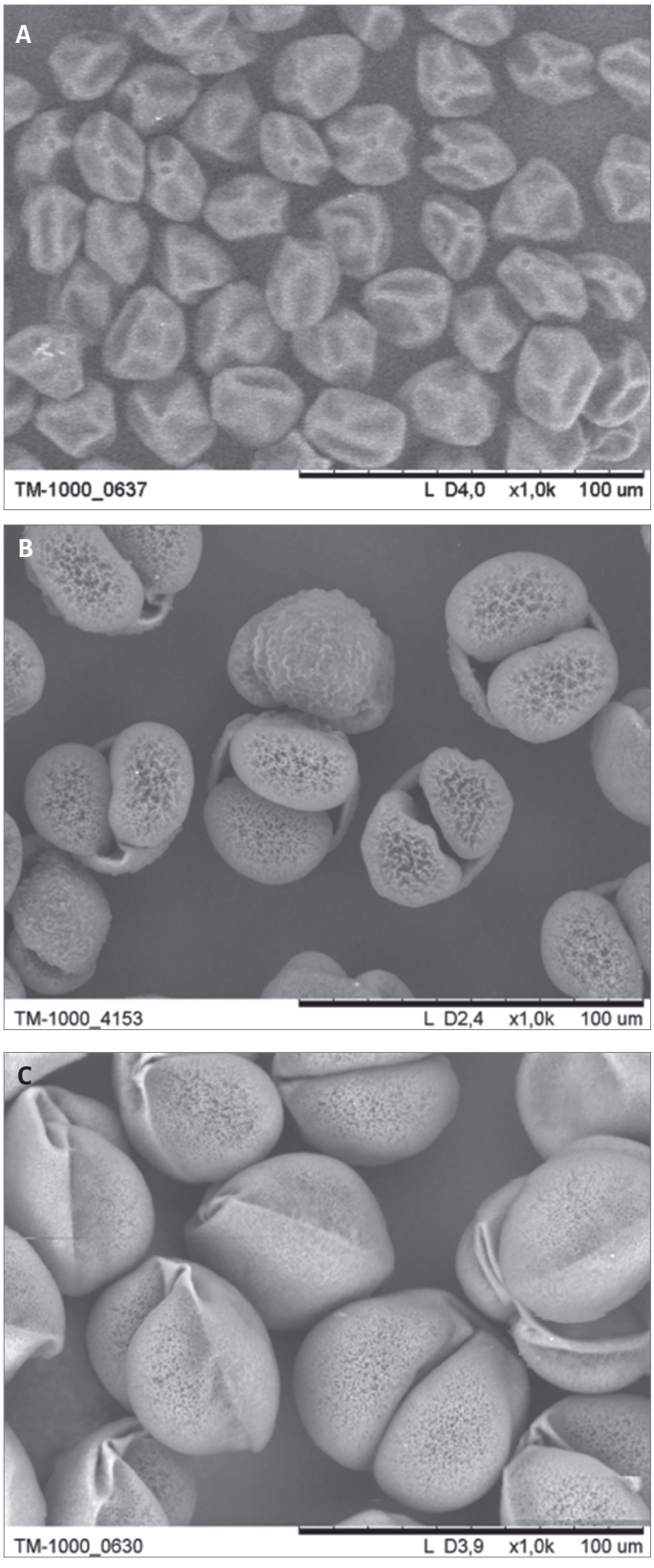

Fig. 4. SEM images of (A) hazel, (B) pine, and (C) spruce pollen grains.

range with a smaller coarse fraction (~120–150 µm) likely representing agglomerates. Hazel pollen, while relatively narrow and centred in the 22–34 µm range, showed slight polydispersity due to occasional larger particles. Pine pollen, based on histogram evaluation, was unimodal and moderately narrow, peaking at

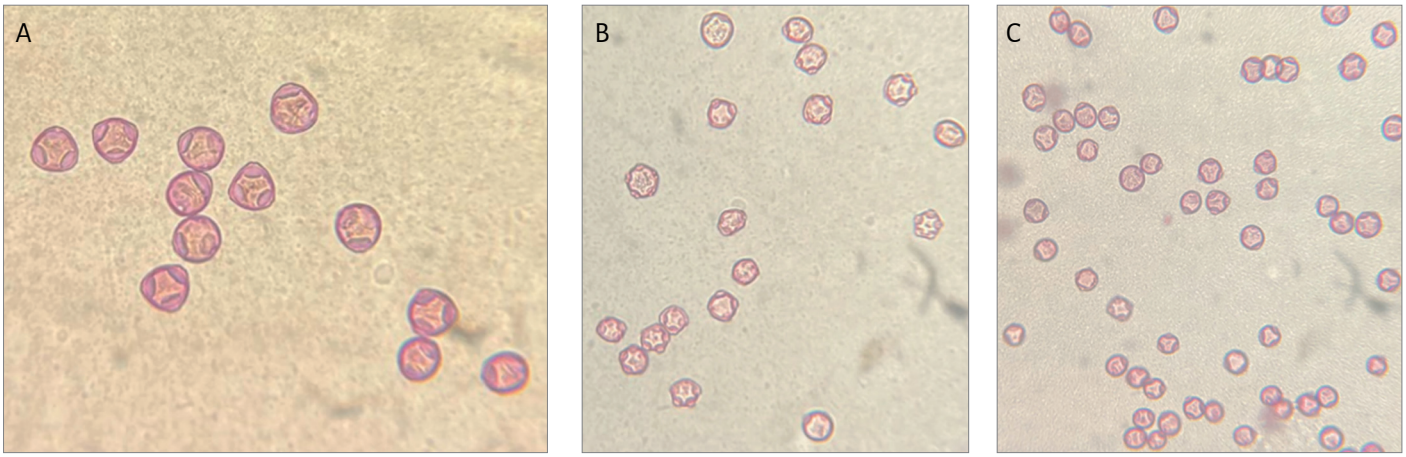

Fig. 5. Pollen images obtained under light microscopy: (A) hazel, (B) alder, (C) birch.

Tab. I. Analysis of birch pollen segmental deposition on a model of the nasal cavity.

AIR FLOW RATE	LOCATION	SEGMENT	MEDIAN [%]	IQR [Q1–Q3]	ANOVA (F, p)
5 L/min	Lateral wall	WA	42.6	[41.3–43.8]	$F(2,9) = 605.8$; $p<0.001$; $\eta^2\approx0.993$
		WM	17.5	[17.4–17.6]	
		WP	9.4	[8.2–10.5]	
	Septum	SA	45.8	[45.2–47.1]	$F(1,6) = 696.7$; $p<0.001$; $\eta^2\approx0.99$
		SP	15.4	[14.8–16.0]	
7.5 L/min	Lateral wall	WA	47.7	[46.7–48.7]	$F(2,9) = 812.5$; $p<0.001$; $\eta^2\approx0.995$
		WM	18.3	[17.2–19.1]	
		WP	8.4	[7.2–9.1]	
	Septum	SA	48.4	[48.0–48.8]	$F(1,6) = 1893$; $p<0.001$; $\eta^2\approx0.998$
		SP	14.2	[13.6–15.1]	
20 L/min	Lateral wall	WA	56.0	[54.8–57.6]	$F(2,9) = 1505$; $p<0.001$; $\eta^2\approx0.998$
		WM	19.0	[18.6–19.4]	
		WP	6.5	[6.4–6.7]	
	Septum	SA	51.4	[51.0–51.9]	$F(1,6) = 1880$; $p<0.001$; $\eta^2\approx0.997$
		SP	16.7	[16.5–17.2]	

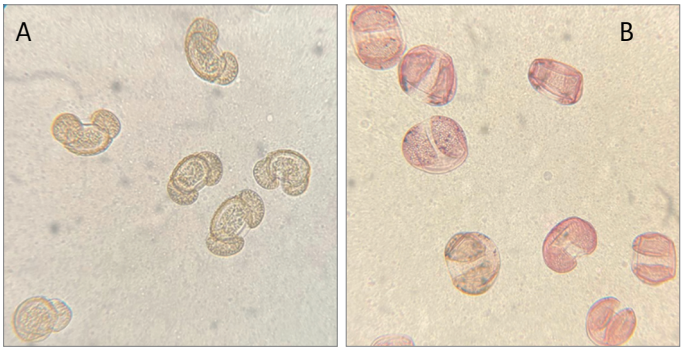

Fig. 6. Pollen images obtained under light microscopy: (A) pine, (B) spruce.

50–60 µm. Spruce pollen had a narrow, unimodal distribution (40–90 µm), characteristic of intact grains with minimal aggregation.

The information on the PSD of aerosolised pollen presented in Fig. 7. is essential for the interpretation of the regional deposition inside the model nasal cavity. The aerosol with the same characteristics is investigated during deposition experiments presented in this work.

Regional pollen deposition based on macroscopic image analysis

An example of a raw photograph of one part of the model (lateral wall) after pollen deposition, with the result of digital image analysis, is shown in Fig. 8.

The cumulative results for each pollen and sediment, both on the lateral wall and nasal septum, along with a statistical analysis of the results, are presented in the following sections. Air flow values reported here are expressed per nostril.

Deposition of birch, alder, and hazel pollen

Analysis of birch, alder, and hazel pollen grains deposition (with diameters ranging from 18 to 34 µm) on the lateral wall of the nasal cavity at each of the specified flow rates (5, 7.5, and 20 L/min per nostril) showed significant differences between the individual segments. While the middle segment (WM), which had the largest surface area, accounted for the largest segment share of the total lateral wall deposition, the highest relative pollen deposition in relation to the segment area

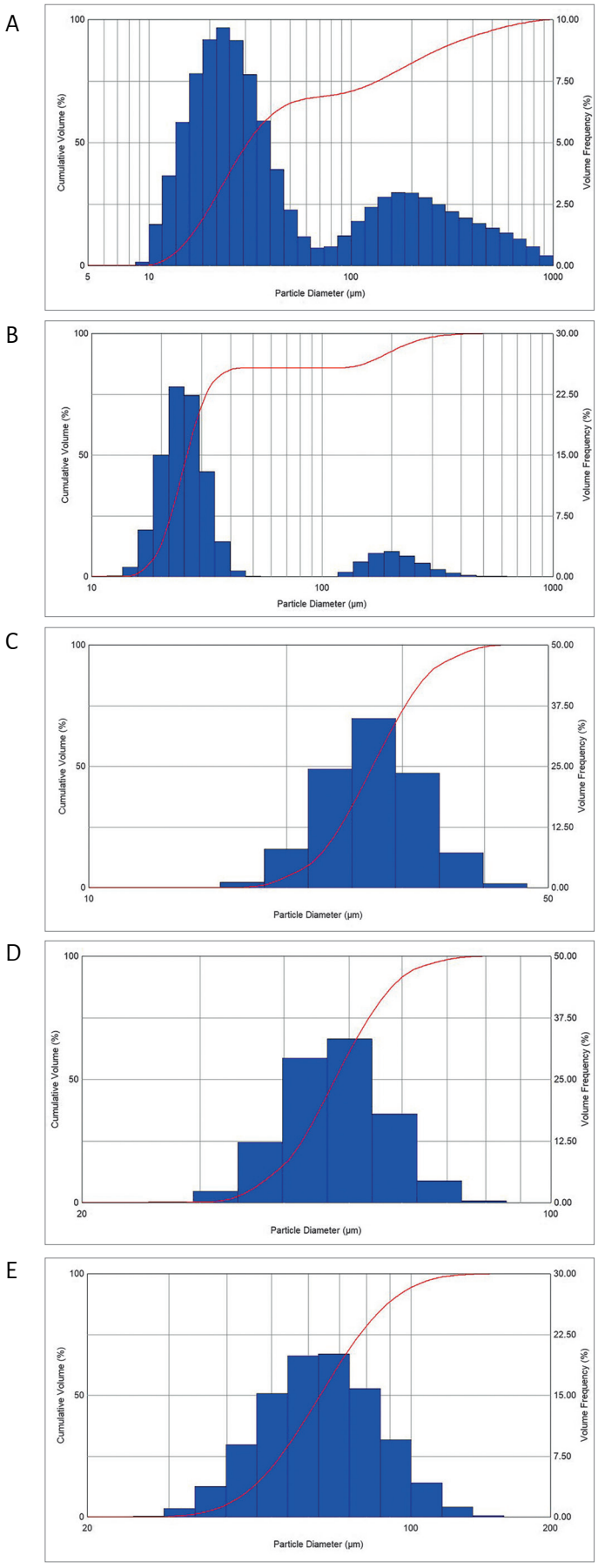

Fig. 7. Particle size distribution of aerosolized pollen: (A) birch, (B) alder, (C) hazel, (D) pine, (E) spruce.



Fig. 8. (A) Macroscopic picture of pine pollen deposition (yellow areas) on the lateral wall and (B) the result of image analysis showing the quantitative data of deposition in three regions: WA, WM, WP. Airflow rate: 20 L/min.

(segmental deposition) was consistently found in the anterior segment (WA). The posterior segment (WP) showed a marginal contribution to the deposition process in each analysis. (Tab. I–III., Fig. 9.–14.).

Lateral wall share % showed an upward trend with increasing air flow through the nasal cavity, reaching the highest values at 20 L/min. As the flow increased (from 5 through 7.5 to 20 L/min), the total amount of deposited pollen increased in both the anterior and middle segments, with a higher flow rate resulting in greater pollen deposition of the anterior segment. Deposition in the posterior segment decreased with increasing flow. The results suggest that intensification of flow rate leads to a shift in the location of maximum deposition towards the anterior sections of the nose, with a simultaneous reduction in pollen penetration into the posterior segments. It is easily explained by an increase in inertial deposition of pollen grains with the increasing air velocity. For aerosol particles of this size (i.e., larger than 20 µm), inertial effects play the key role in the deposition in the nasal cavity. According to this mechanism, a particle cannot follow the abrupt change in the direction of airflow and impacts the obstacle (here: the surface of the nasal wall or septum). A more detailed explanation of this, as well as other mechanisms responsible for pollen deposition in the nasal cavity, is presented in the Discussion.

Observations on the deposition of birch, alder, and hazel pollen grains on the nasal septum indicate significant spatial variation in grain deposition at each airflow rate analysed. For all tested flows, the largest percentage of the segment area covered with pollen was recorded in the anterior segment (SA). Still, the posterior

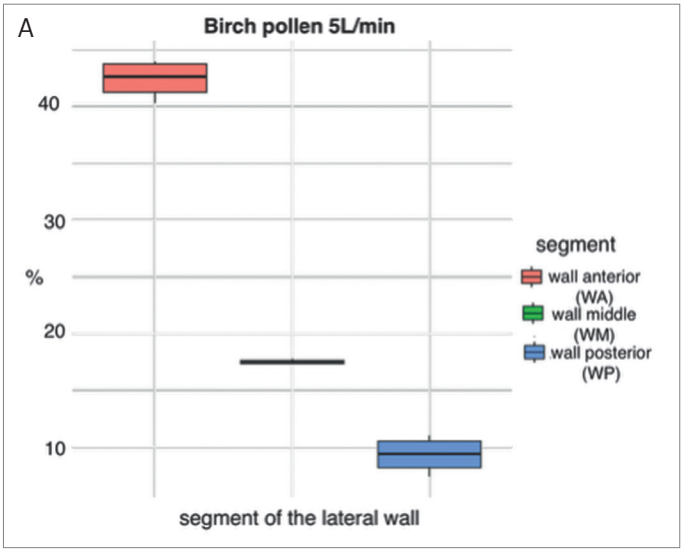

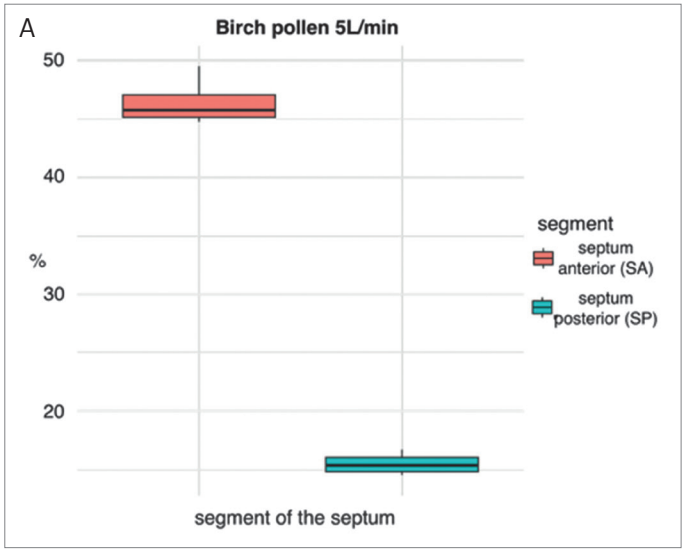

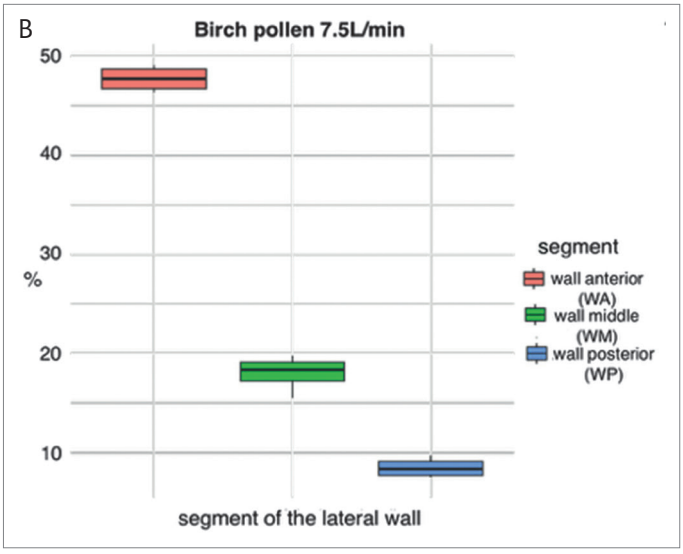

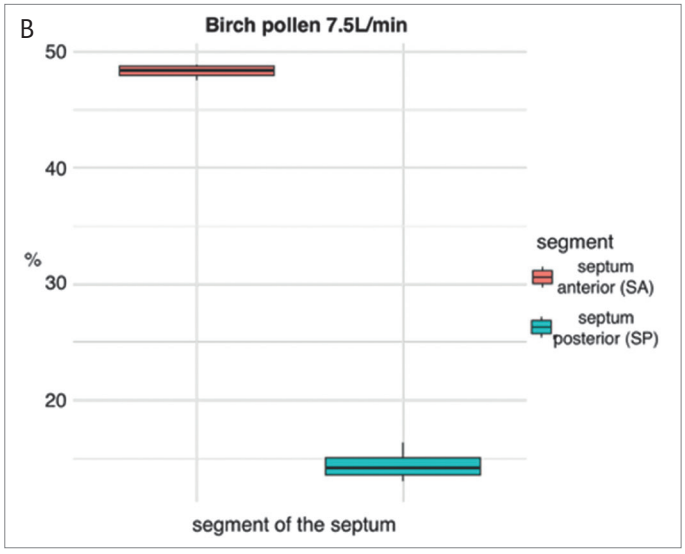

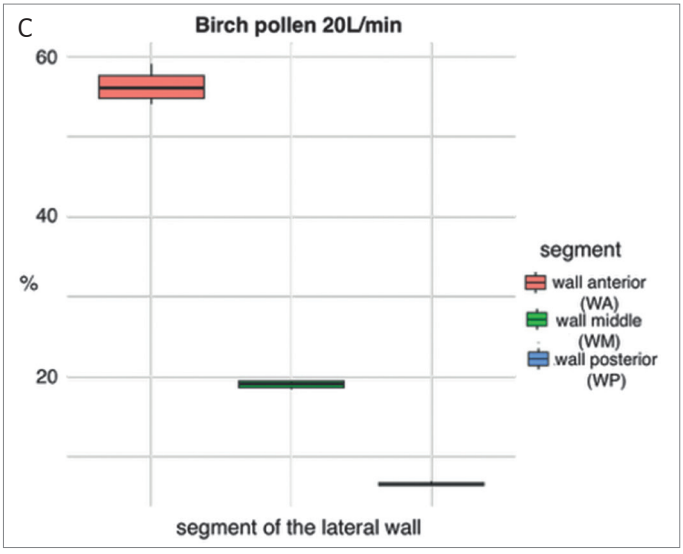

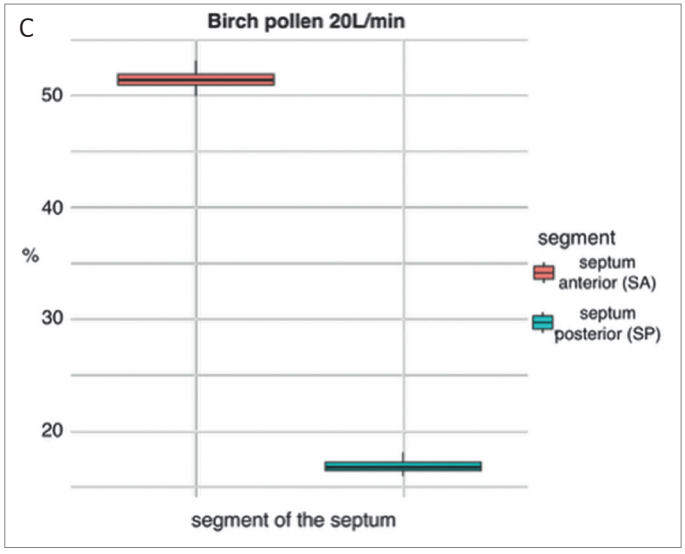

Fig. 9. Birch pollen segmental deposition on the lateral wall of the nasal cavity at a flow rate of (A) 5 L/min, (B) 7.5 L/min, (C) 20 L/min.

Fig. 10. Birch pollen segmental deposition on the nasal septum at flow rates of (A) 5 L/min, (B) 7.5 L/min, (C) 20 L/min.

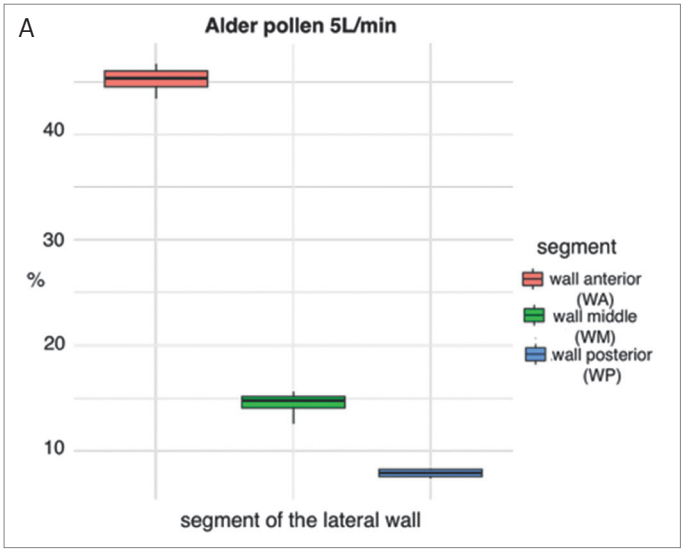

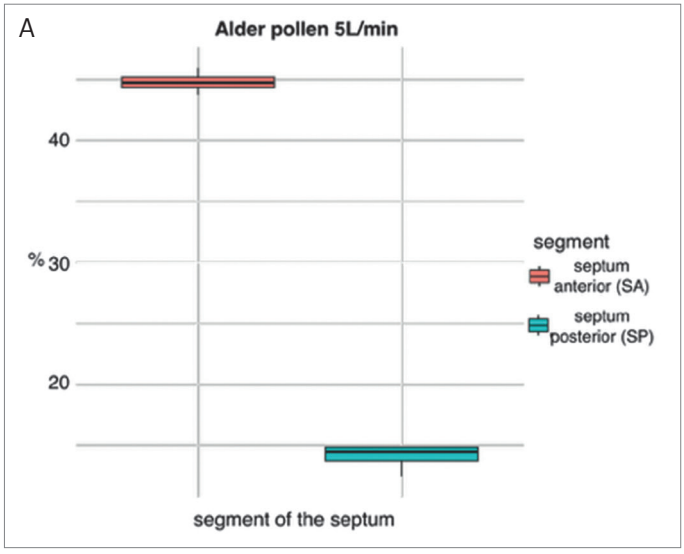

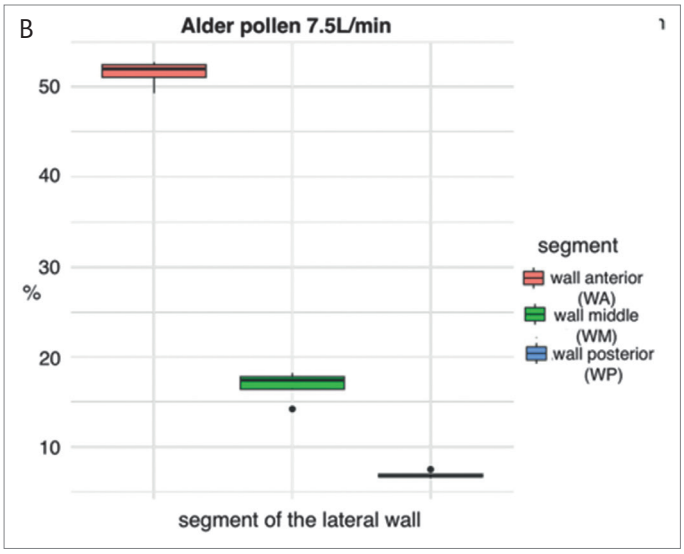

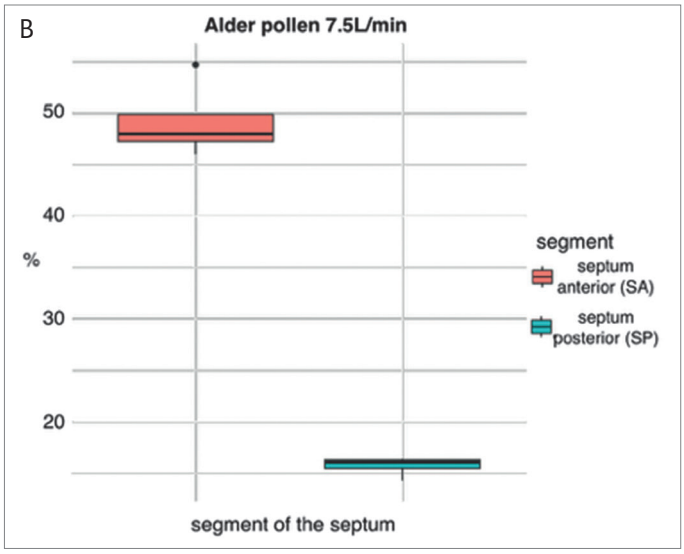

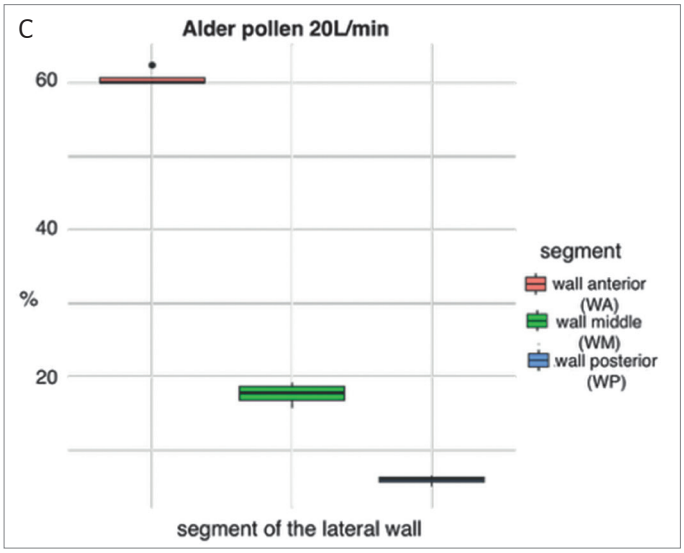

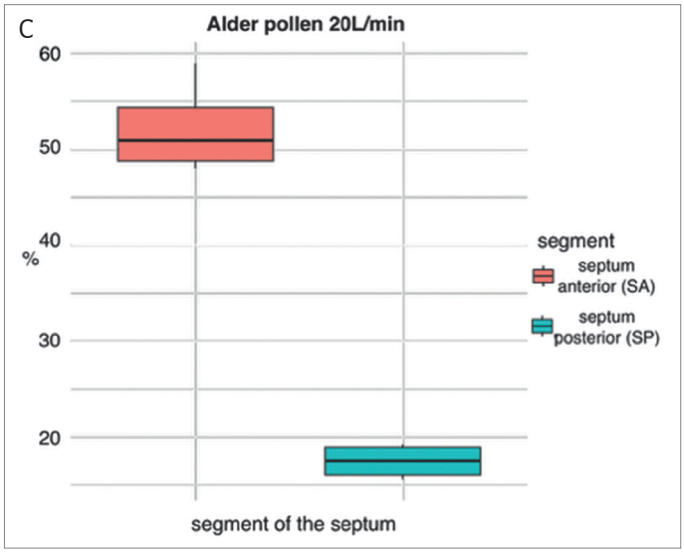

Fig. 11. Alder pollen segmental deposition on the lateral wall of the nasal cavity at a flow rate of (A) 5 L/min, (B) 7.5 L/min, (C) 20 L/min.

Fig. 12. Alder pollen segmental deposition on the nasal septum at flow rates of (A) 5 L/min, (B) 7.5 L/min, (C) 20 L/min.

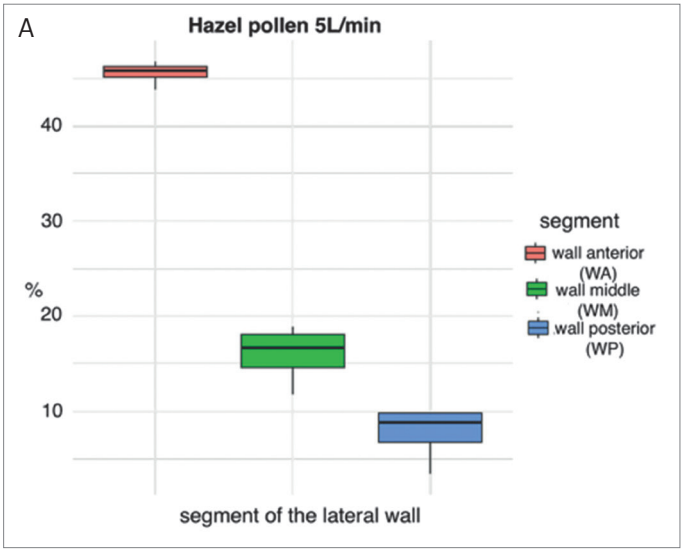

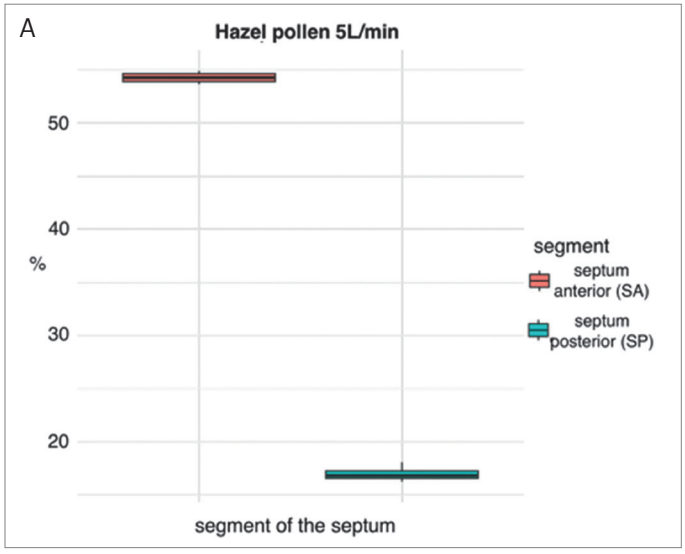

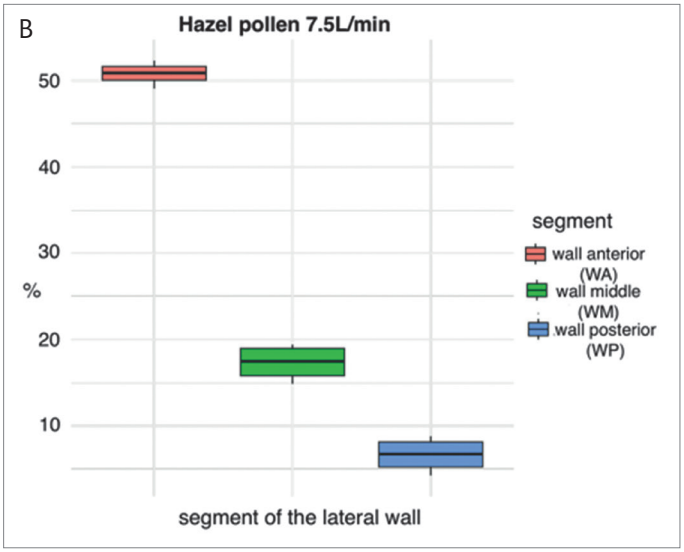

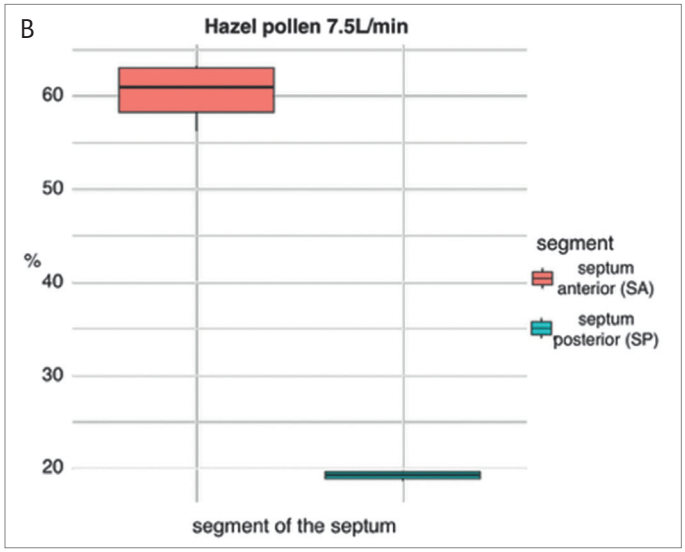

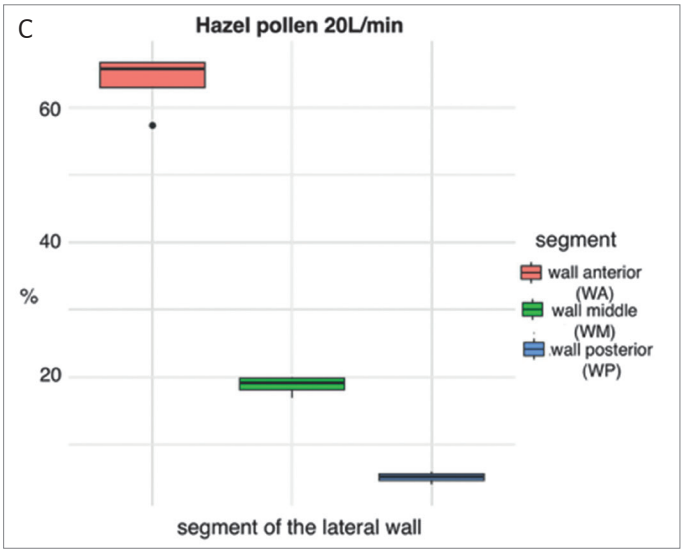

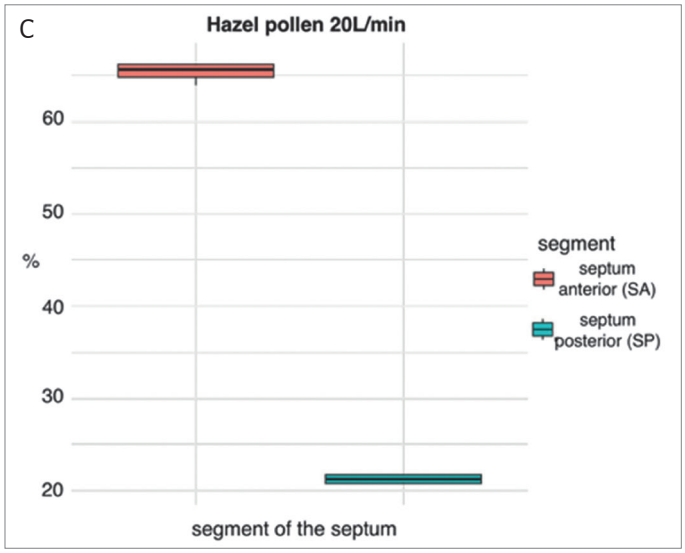

Fig. 13. Hazel pollen segmental deposition on the lateral wall of the nasal cavity at a flow rate of (A) 5 L/min, (B) 7.5 L/min, (C) 20 L/min.

Fig. 14. Hazel pollen segmental deposition on the nasal septum at flow rates of (A) 5 L/min, (B) 7.5 L/min, (C) 20 L/min.

Tab. II. Analysis of alder pollen segmental deposition on a model of the nasal cavity.

AIR FLOW RATE	LOCATION	SEGMENT	MEDIAN [%]	IQR [Q1–Q3]	ANOVA (F, p)
5 L/min	Lateral wall	WA	45.4	[44.5–46.0]	F(2,9) = 1208; p<0.001; η^2≈0.997
		WM	14.8	[14.1–15.1]	
		WP	7.9	[7.5–8.2]	
	Septum	SA	44.7	[44.4–45.2]	F(1,6) = 1748; p<0.001; η^2≈0.997
		SP	14.5	[13.7–14.9]	
7.5 L/min	Lateral wall	WA	52.0	[51.1–52.5]	F(2,9) = 1142; p<0.001; η^2≈0.997
		WM	17.4	[16.4–17.8]	
		WP	6.8	[6.7–7.0]	
	Septum	SA	48.0	[47.3–49.9]	F(1,6) = 288.6; p<0.001; η^2≈0.98
		SP	16.1	[15.5–16.3]	
20 L/min	Lateral wall	WA	60.0	[59.8–60.2]	F(2,9) = 2419; p<0.001; η^2≈0.998
		WM	17.8	[16.8–18.7]	
		WP	6.0	[5.7–6.3]	
	Septum	SA	50.9	[48.8–54.3]	F(1,6) = 172.9; p<0.001; η^2≈0.97
		SP	17.5	[16.1–18.9]	

Tab. III. Analysis of hazel pollen segmental deposition on a model of the nasal cavity.

AIR FLOW RATE	LOCATION	SEGMENT	MEDIAN [%]	IQR [Q1–Q3]	ANOVA (F, p)
5 L/min	Lateral wall	WA	45.8	[45.1–46.2]	F(2,9)=230.6; p<0.001; η^2≈0.98
		WM	16.7	[14.6–18.1]	
		WP	8.8	[6.7–9.8]	
	Septum	SA	54.3	[53.9–54.6]	F(1,6)=5891; p<0.001; η^2≈0.999
		SP	16.8	[16.6–17.3]	
7.5 L/min	Lateral wall	WA	50.9	[50.1–51.7]	F(2,9)=578.5; p<0.001; η^2≈0.993
		WM	17.5	[15.8–19.0]	
		WP	6.7	[5.2–8.1]	
	Septum	SA	61.0	[58.3–63.1]	F(1,6)=582.7; p<0.001; η^2≈0.991
		SP	19.3	[18.9–19.7]	
20 L/min	Lateral wall	WA	65.8	[63.0–66.7]	F(2,9)=503.3; p<0.001; η^2≈0.991
		WM	19.2	[18.1–19.9]	
		WP	5.2	[4.7–5.6]	
	Septum	SA	65.7	[64.8–66.2]	F(1,6)=1880; p<0.001; η^2≈0.991
		SP	21.7	[20.8–21.7]	

segment (SP) contributed more to the segment share of total septal deposition (the septal share %) due to its larger surface area. The value increased with air flow. The segmental deposition values did not differ significantly between flows (p< 0.05), with a slight upward trend in the anterior segment at higher flows.

The medians and IQR-interquartile range [Q1–Q3] of birch, alder, and hazel pollen grain fractions relative to the surface area of individual segments of the lateral wall and septum of the nasal cavity (% of the segment's surface area covered with pollen) are presented in Tab. I.–III. They also show the results of one-way ANOVA analyses, which were confirmed by the Kruskal-Wallis test (p = 0.007 for the lateral wall; p = 0.021 for the septum in the case of each pollen type), which proves the consistency of the results regardless of the type of analysis. Paired samples t-tests confirmed that deposition in the anterior segment (WA) was significantly higher than in the middle (WM) and posterior (WP) segments for all analysed pollen types (birch, alder, hazel) and flow rates. For birch, the WA–WM/WA–WP differences were 0.25/0.33 at 5 L/min, 0.30/0.39 at 7.5 L/min, and 0.37/0.50 at 20 L/min, respectively. For alder, values increased significantly (ANOVA test, p<0.001), reaching 0.31/0.37 (5 L/min), 0.35/0.45 (7.5 L/min), and 0.43/0.55 (20 L/min), respectively. For hazel, the differences were particularly pronounced at the highest flow rate: 0.45 (WA–WM) and 0.59 (WA–WP). The differences between the WA–WM and WA–WP segment values increased significantly (ANOVA test, p<0.001) with the intensity of the flow.

INDEX COPERNICUS INTERNATIONAL

Tab. IV. Analysis of pine pollen segmental deposition on a model of the nasal cavity.

AIR FLOW RATE	LOCATION	SEGMENT	MEDIAN [%]	IQR [Q1–Q3]	ANOVA (F, p, η^2)
5 L/min	Lateral wall	WA	62.4	[61.6–63.2]	F(2,9) = 2013; p<0.001; η^2=0.998
		WM	14.8	[14.0–15.7]	
		WP	5.5	[5.1–5.7]	
	Septum	SA	63.5	[62.7–64.8]	F(1,6) = 2331; p<0.001; η^2≈0.997
		SP	12.2	[11.9–12.7]	
7.5 L/min	Lateral wall	WA	70.1	[69.6–70.7]	F(2,9) = 6211; p<0.001; η^2=0.999
		WM	15.9	[15.4–16.3]	
		WP	4.7	[4.6–4.8]	
	Septum	SA	68.3	[67.9–68.6]	F(1,6) = 7640; p<0.001; η^2≈0.999
		SP	13.5	[12.9–14.2]	
20 L/min	Lateral wall	WA	79.1	[77.8–80.1]	F(2,9) = 3503; p<0.001; η^2=0.999
		WM	16.8	[16.3–17.3]	
		WP	3.6	[3.4–3.9]	
	Septum	SA	72.9	[68.2–77.0]	F(1,6) = 279.2 ; p<0.001; η^2≈0.999
		SP	14.5	[14.0–15.1]	

Tab. V. Analysis of spruce pollen segmental deposition on a model of the nasal cavity.

AIR FLOW RATE	LOCATION	SEGMENT	MEDIAN [%]	IQR [Q1–Q3]	ANOVA (F, p, η^2)
5 L/min	Lateral wall	WA	63.4	[61.5–64.1]	F(2,9) = 1120; p<0.001; η^2≈0.997
		WM	14.7	[14.1–15.7]	
		WP	3.6	[3.5–4.0]	
	Septum	SA	65.4	[62.4–67.8]	F(1,6) = 461; p<0.001; η^2≈0.99
		SP	13.6	[12.8–14.3]	
7.5 L/min	Lateral wall	WA	71.4	[69.2–71.8]	F(2,9) = 764.4; p<0.001; η^2≈0.99
		WM	15.5	[14.9–16.7]	
		WP	3.2	[3.1–3.4]	
	Septum	SA	69.1	[65.7–72.5]	F(1,6) = 450; p<0.001; η^2≈0.99
		SP	14.1	[13.9–14.6]	
20 L/min	Lateral wall	WA	76.5	[75.8–77.9]	F(2,9) = 164; p<0.001; η^2≈0.99
		WM	17.3	[15.7–18.9]	
		WP	2.5	[2.3–3.0]	
	Septum	SA	74.8	[72.5–77.3]	F(1,6) = 716; p<0.001; η^2≈0.99
		SP	15.2	[15.0–15.7]	

When the segmental deposition of birch pollen grains was related to the entire surface area of the lateral wall of the nasal cavity, so that it represents the percentage of the entire lateral wall covered by pollen assigned to a given segment (area-weighted), then at a flow rate of 5 L/min, it corresponded to a coverage of 7.8% [7.6–8.0] of the surface area in the anterior segment (WA), 11.5% [11.4–11.6] in the middle segment (WM), and 1.5% [1.3–1.7] in the posterior segment (WP), while at a flow rate of 7.5 L/min, it corresponded to 8.7% [8.6–8.9] of the surface area in the anterior segment (WA), 12.1% [11.3–12.6] in the middle (WM), and only 1.3% [1.2–1.5] in the posterior (WP), while at a flow rate of 20 L/min – 10.3% [10.0–10.5] of the surface area in the anterior segment (WA), 12.5% [12.2–12.7] in the middle (WM), and 1.1% [1.0–1.1] in the posterior (WP) segment.

When the birch pollen segmental deposition in individual segments of the septum was related to its total surface area, the following values were obtained: at a flow rate of 5 L/min – SA: 9.9% [9.8–10.1] of the septum surface area, SP: 11.4% [10.6–11.8]; at a flow rate of 7.5 L/min – SA: 10.6% [10.5–10.6], SP: 11.1% [10.6–11.8]; and at a flow rate of 20 L/min – SA: 11.2% [11.1–11.3], SP: 13.1% [12.6–13.4].

When the segmental deposition of alder pollen grains was related to the entire lateral wall surface at a flow rate of 5 L/min, it corresponded to a coverage of 8.3% [8.1–8.4] of the surface in the front segment (WA), 9.7% [9.2–9.9] in the middle segment (WM), and 1.3% [1.2–1.3] in the posterior segment (WP), at a flow rate of 7.5 L/min – 9.5% [9.3–9.6] of the surface area in the front segment (WA), 11.4% [10.8–11.7] in the middle (WM), and only 1.08% [1.07–1.12] in the posterior (WP), while at a flow rate of 20 L/min – 11.0% [11.0–11.1] of the surface area in the anterior segment (WA), 11.7% [11.0–12.3] in the middle segment (WM) and 1.0% [0.9–1.0] in the posterior segment (WP).

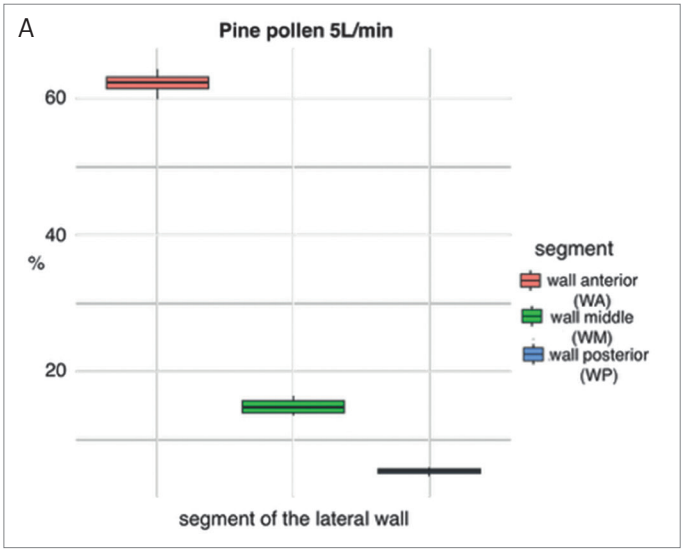

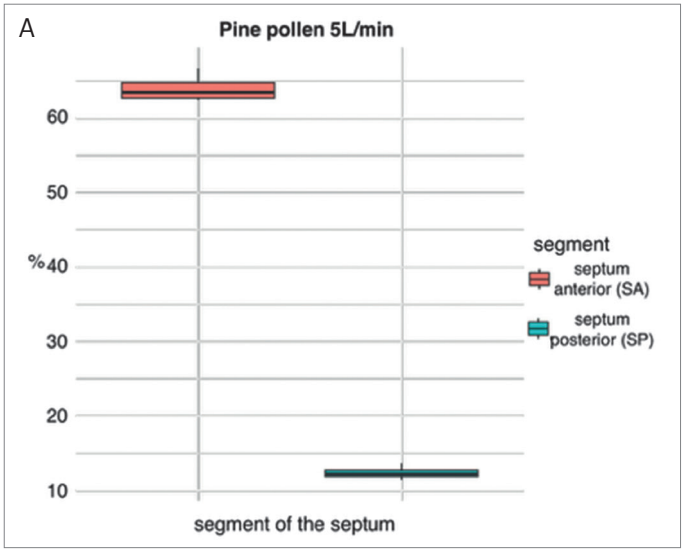

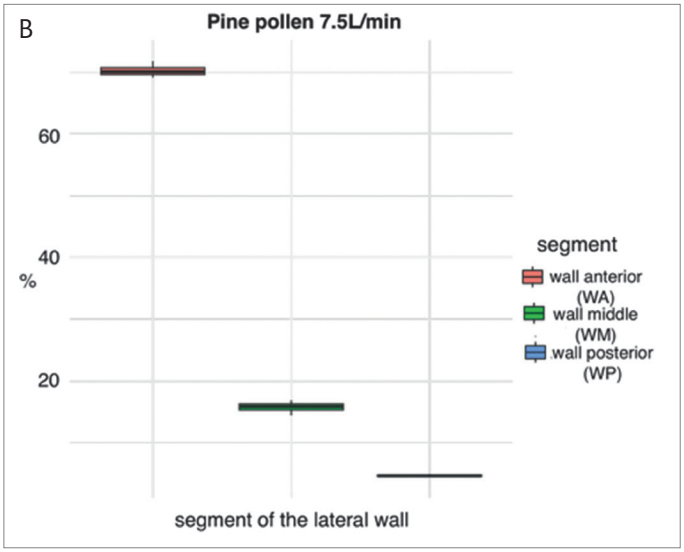

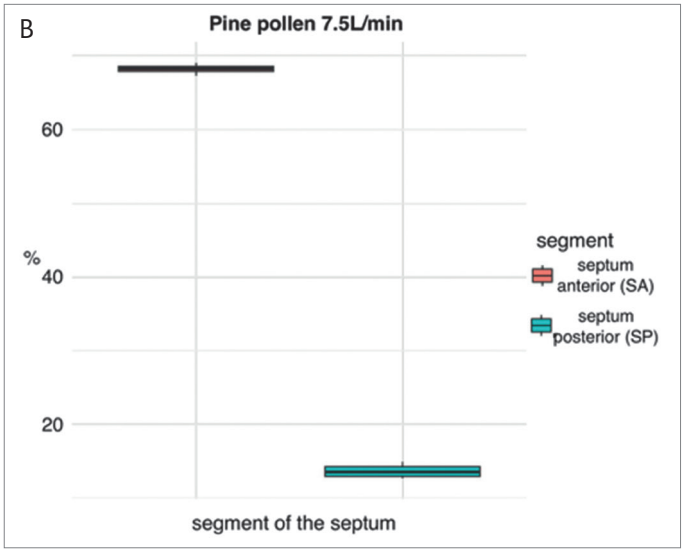

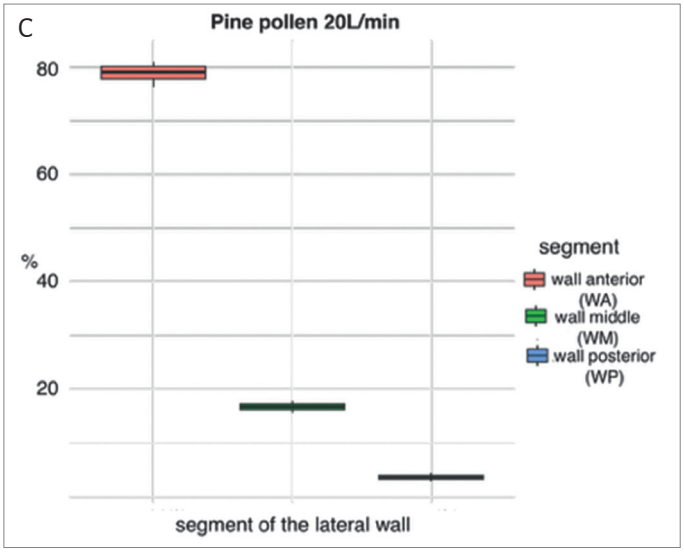

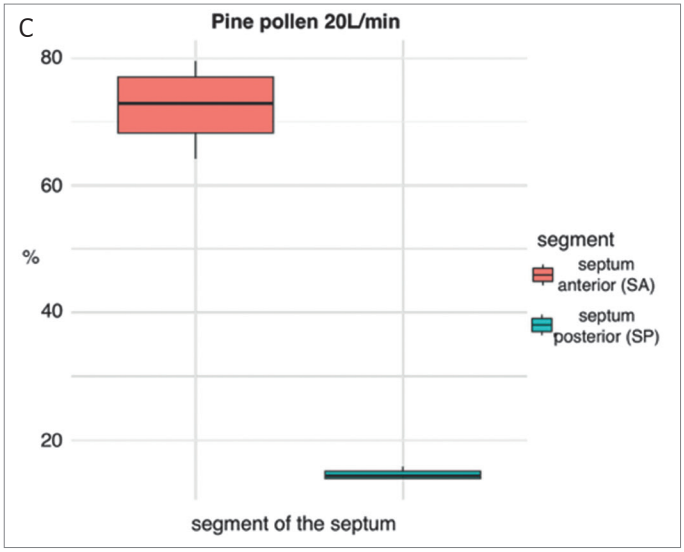

Fig. 15. Pine pollen segmental deposition on the lateral wall of the nasal cavity at a flow rate of (A) 5 L/min, (B) 7.5 L/min, (C) 20 L/min.

Fig. 16. Pine pollen segmental deposition on the nasal septum at flow rates of (A) 5 L/min, (B) 7.5 L/min, (C) 20 L/min.

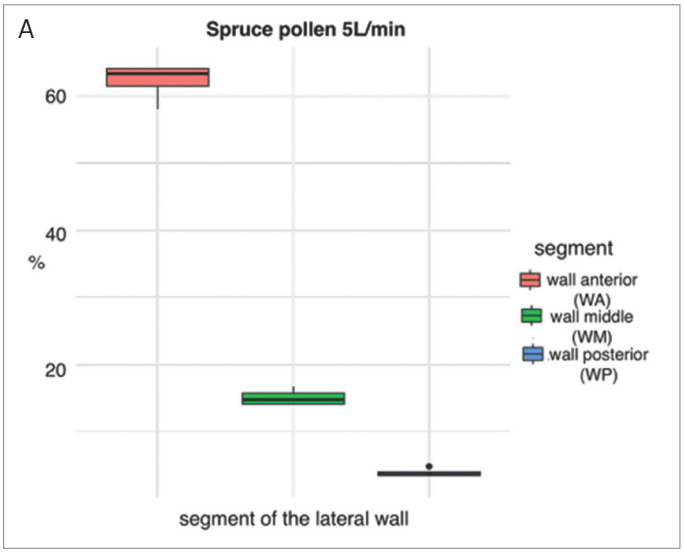

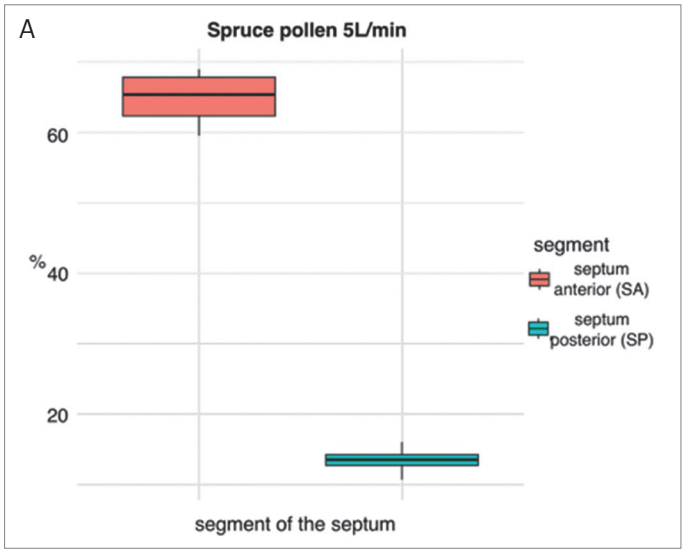

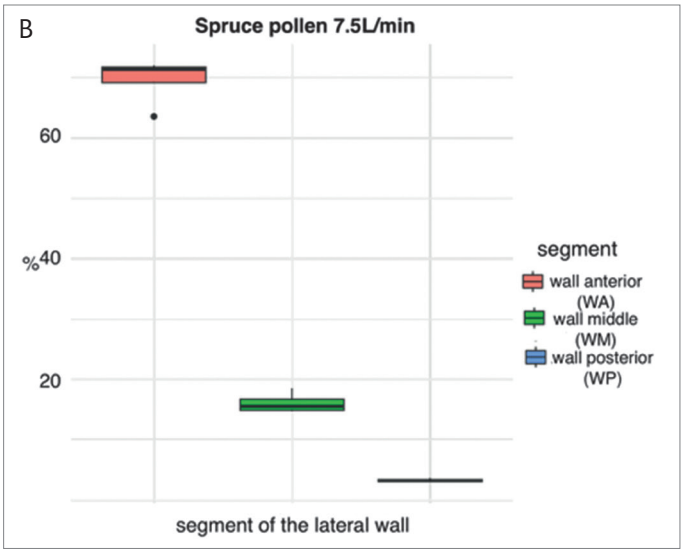

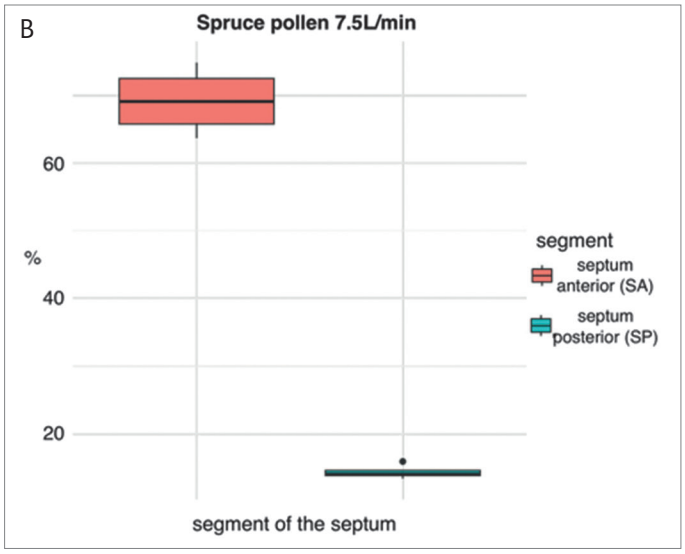

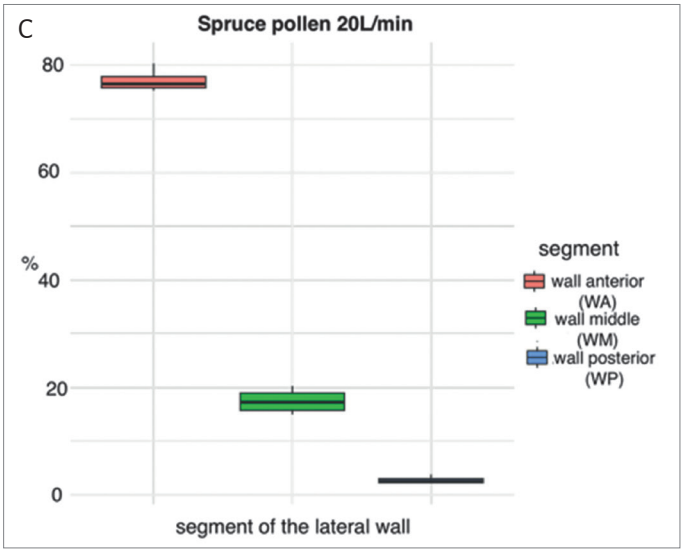

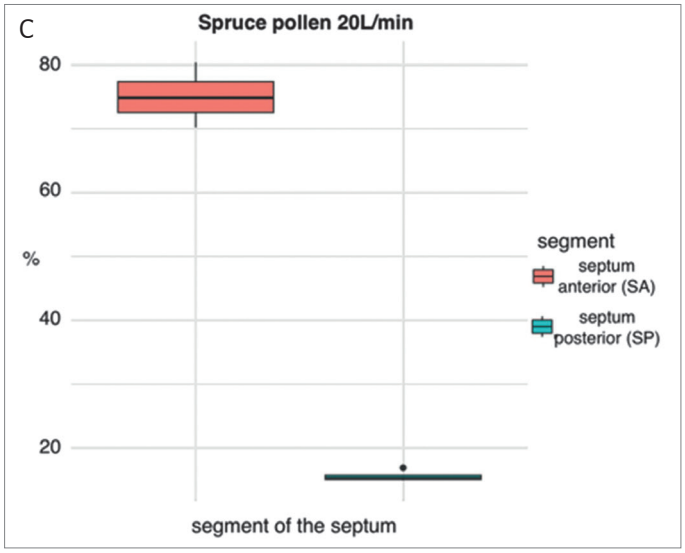

Fig. 17. Spruce pollen segmental deposition on the lateral wall of the nasal cavity at a flow rate of (A) 5 L/min, (B) 7.5 L/min, (C) 20 L/min.

Fig. 18. Spruce pollen segmental deposition on the nasal septum at flow rates of (A) 5 L/min, (B) 7.5 L/min, (C) 20 L/min.

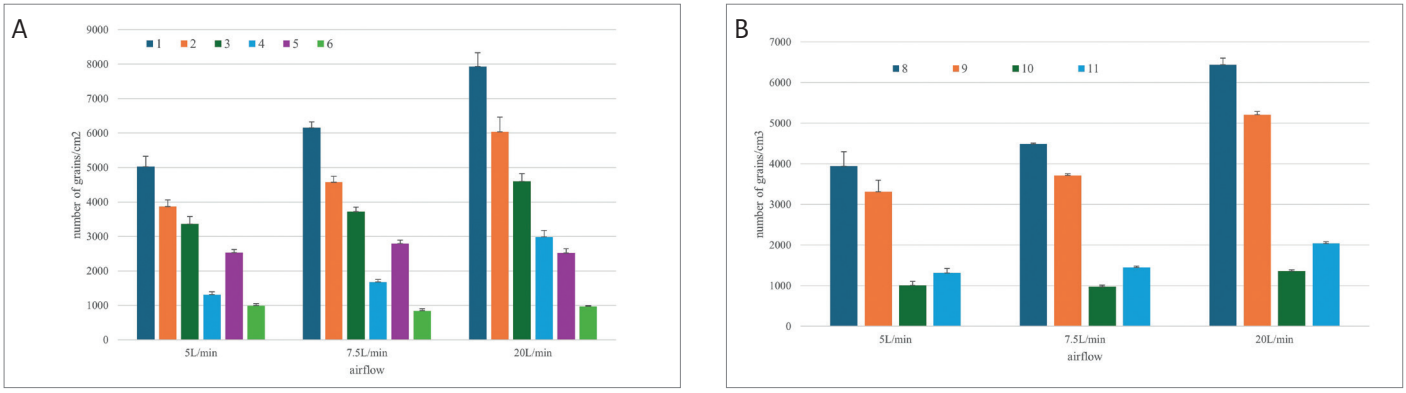

Fig. 19. Regional deposition of birch pollen (locations 1–11) based on microscopic evaluation of slides on the lateral wall (A) and nasal septum (B) at different flow rates.

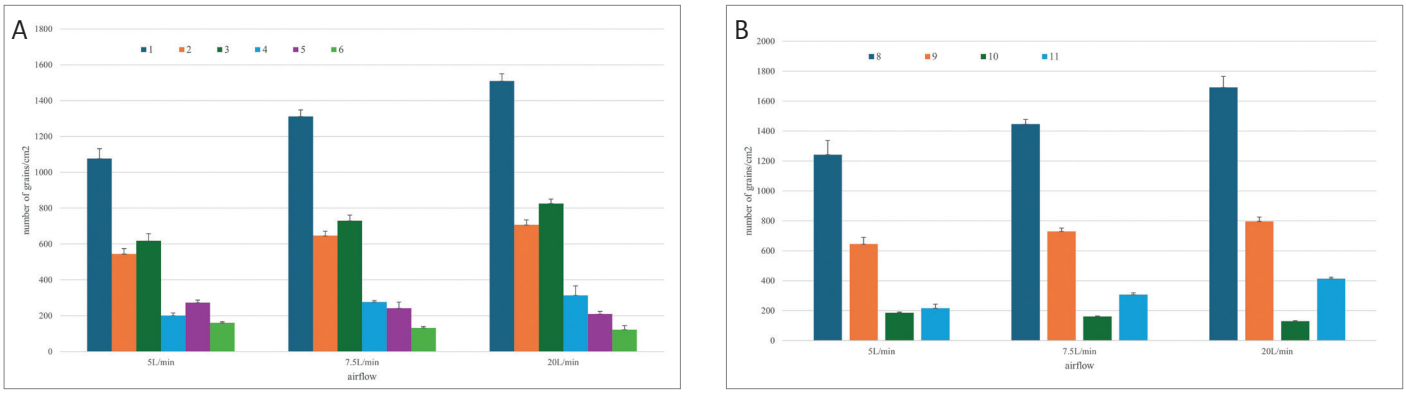

Fig. 20. Regional deposition of pine pollen (locations 1–11) based on microscopic evaluation of slides on the lateral wall (A) and nasal septum (B) at different flow rates.

When the deposition of alder pollen in individual segments of the septum was related to its total surface area, the following values were obtained: at a flow rate of 5 L/min – SA: 9.8% [9.7–9.9] of the septum surface area, SP: 11.3% [10.7–11.6]; at a flow rate of 7.5 L/min – SA: 10.5% [10.3–10.9], SP: 12.6% [12.1–12.7]; and at a flow rate of 20 L/min – SA: 11.1% [10.6–11.8], SP: 13.7% [12.6–14.8].

After relating the segmental pollen deposition values for hazel pollen to the entire lateral wall surface at a flow rate of 5 L/min, this corresponded to a coverage of 8.4% [8.3–8.5] of the surface in the front segment (WA), 11.0% [9.6–11.9] in the middle segment (WM), and 1.4% [1.1–1.6] in the posterior segment (WP), at a flow rate of 7.5 L/min – 9.3% [9.2–9.5] of the surface area in the front segment (WA), 11.5% [10.4–12.5] in the middle (WM) and only 1.1% [0.8–1.3] in the posterior (WP), while at a flow rate of 20 L/min – 12.0% [11.5–12.2] of the surface area in the anterior segment (WA), 12.6% [11.9–13.1] in the middle (WM) and 0.8% [0.8–0.9] in the posterior segment (WP).

After relating the deposition of hazel pollen in individual segments of the septum to its total surface area, the following values were obtained: at a flow rate of 5 L/min – SA: 11.8% [11.7–11.9] of the septum surface, SP: 13.2% [12.0–13.5]; at a flow rate of 7.5 L/min – SA: 13.3% [12.7–13.7], SP: 15.1% [14.8–15.4]; and at a flow rate of 20 L/min – SA: 14.3% [14.1–14.4], SP: 16.6% [16.3–17.0].

Pine and spruce pollen deposition

The values of segmental pollen deposition in the anterior segment were significantly (ANOVA test, $p<0.001$) higher than in the middle (WM) and posterior (WP) segments. An increase in flow to 20 L/min intensified the accumulation of pine pollen grains in the anterior segment, maintaining this part as the primary site of both segmental deposition and lateral wall share %. At each flow rate, most of the large spruce pollen grains were deposited in the anterior part of the lateral wall; at 7.5 L/min, they covered more than 2/3 of its surface, and at 20 L/min, almost 4/5. In contrast, the posterior segment was almost absent from the deposition at each of the analysed flow rates (Tab. IV.–V., Fig. 15.–18.).

The segment share of total lateral wall deposition (lateral wall share %) increased with the air flow in the nasal cavity. For spruce pollen, the share of the anterior segment increased from 11.6% (5 L/min) to 14.0% (20 L/min). In comparison, the middle segment WM showed only a slight increase in deposition (9.7% → 11.3%), and the posterior segment WP showed a decrease (0.6% → 0.4%). Even with intense inhalation, < 1% of the lateral wall share % was in the posterior segment WP, suggesting that large grains are unable to reach the posterior part of the lateral wall at any of the tested flow rates.

For each of the analysed flow rates, the deposition of pine and spruce pollen on the nasal septum of adults was significantly greater in the anterior segment (SA) than in the posterior segment (SP). At a flow rate of 20 L/min, the vast majority of particles (>70%) were deposited in the anterior part of the nasal septum, while the posterior segment accumulated several times less. An increase in flow rate increased the septal share % in both segments. Still, it did not change the hierarchy – the anterior segment remained the dominant site of deposition, and the segment effect was very strong ($\eta^2>0.99$).

The medians and IQR [Q1–Q3] of pine and spruce pollen grain fractions related to the surface area of individual segments of the lateral wall and nasal septum (% of segment surface area covered with pollen) are presented in Tab. IV.–V. They also show the results of one-way ANOVA analyses, which were confirmed by the Kruskal--Wallis test ($p = 0.007$ for the lateral wall; $p = 0.021$ for the septum in the case of both plants), which proves the consistency of the results regardless of the type of analysis. Paired samples t-tests for pine pollen deposition showed significantly higher deposition in the front segment (WA) compared to the middle (WM) and posterior (WP) segments for all flows. At 5 L/min, the WA–WM and WA–WP differences were 0.47 and 0.57, respectively, at 7.5 L/min – 0.54 and 0.66, and at 20 L/min – 0.62 and 0.75. Similarly, for spruce, deposition in the WA segment was significantly higher than in WM and WP. At a flow rate of 5 L/min, the differences were 0.47 and 0.58, respectively, at 7.5 L/min – 0.54 and 0.66, and at 20 L/min – 0.60 and 0.74.

When the segmental deposition value of pine pollen grains was related to the entire lateral wall surface at a flow rate of 5 L/min, it corresponded to a coverage of 11.4% [11.2–11.6] of the surface in the anterior segment (WA), 9.7% [9.2–10.3] in the middle segment (WM) and 0.9% [0.8–0.9] in the posterior segment (WP), at a flow rate of 7.5 L/min – 12.8% [12.7–12.9] of the surface area in the front segment (WA), 10.4% [10.1–10.7] in the middle (WM) and only 0.7% [0.7–0.8] in the posterior (WP), while at a flow rate of 20 L/min – 14.5% [14.2–14.7] of the surface area in the anterior segment (WA), 11.0% [10.7–11.6] in the middle (WM) and 0.6% [0.5–0.6] in the posterior (WP) segment.

After relating the deposition of pine pollen in individual segments of septum to its total surface area, the following values were obtained: at a flow rate of 5 L/min – SA: 13.8% [13.7–14.1] of the septum surface area, SP: 9.5% [9.3–9.9]; 7.5 L/min – SA: 14.9% [14.8–15.0], SP: 10.6% [10.1–11.1]; 20 L/min – SA: 15.9% [14.9–16.8], SP: 11.3% [11.0–11.8].

When the segmental deposition value of spruce pollen grains was related to the entire lateral wall at a flow rate of 5 L/min, it corresponded to a coverage of 11.6% [11.3–11.7] of the area in the anterior segment (WA), 9.7% [9.3–10.3] in the middle segment (WM), and 0.6% [0.55–0.63] in the posterior segment (WP), at a flow rate of 7.5 L/min – 13.1% [12.7–13.1] of the surface area in the anterior segment (WA), 10.2% [9.8–11.0] in the middle segment (WM), and only 0.5% [0.49–0.54] in the posterior segment (WP), while at a flow rate of 20 L/min – 14.0% [13.9–14.3] of the surface area in the anterior segment (WA), 11.3% [10.3–12.4] in the middle segment (WM), and 0.4% [0.36–0.48] in the posterior segment (WP).

After relating the deposition of spruce pollen in individual segments of the septum to its total surface area, the following values were obtained: at a flow rate of 5 L/min – SA: 14.2% [13.6–14.8] of the septum surface area, SP: 10.6% [10.0–11.2]; 7.5 L/min – SA: 15.1% [14.3–15.8], SP: 11.0% [10.8–11.4]; 20 L/min – SA: 16.3% [15.8–16.9], SP: 11.9% [11.8–12.3].

Regional pollen deposition based on the microscopic evaluation of slides

Regardless of pollen type (birch, alder, hazel, pine, spruce), the highest deposition on the lateral wall of the nasal cavity was observed in region 1, followed by regions 2 and 3, and the lowest in region 6. Region 4 was characterised by intermediate deposition, while regions 5–6 showed significantly lower deposition. The average between regions increased with increasing flow for all pollen types tested (+10–55% at 20 *vs* 5 L/min). The increase was mainly due to deposition in regions 1–4 (monotonic trend 5 → 7.5 → 20 L/min), while regions 5–6 often gained or lost. The effect of flow rate change is significant in the context of deposition on the lateral wall of the nasal cavity, but less than the variation between wall regions (Fig. 19.–20.).

For all pollen species, the highest deposition on the nasal septum was observed in region 8, followed by region 9, intermediate in region 11, and the lowest in region 10. The interregional average also increased with increasing flow rate (range +16–57% at 20 *vs* 5 L/min; usually a monotonic trend). Regions 8, 9, and 11 mostly increased deposition with the flow rate. In contrast, deposition in region 10 increased for alder, hazel, and birch, but decreased for pine and spruce at higher flow rates.

DISCUSSION

The nasal passages act as an effective filter for inhaled particles. Both experimental studies using in vivo methods and replicas of nasal casts [16, 18, 27, 31–34] as well as studies based on CFD technology used to measure filtration efficiency and particle deposition in the human nose have been published, with the latter being more widely available [14–17, 31–33, 35–40]. Overall, good agreement was observed between CFD predictions and experimental measurements with similar deposition trends in each region of interest. Geometric differences between CFD models and physical replicas of the nose are believed to be the main reasons for potential discrepancies between computational predictions and experimental measurements of particle deposition, particularly in terms of the texture and smoothness of the nose surface [32, 35]. Liu et al. used both experimental measurements in a replica cast and CFD simulations to analyse regional deposition in a nasal cavity model, observing good agreement between experimental measurements and computational modelling, with a slight underestimation of the data by the CFD model in the anterior region [31]. In the study by Shen et al., the agreement between CFD simulations and experimental evaluations on a nasal replica depended on particle size, being excellent for large particles and monodisperse systems, and somewhat limited for complex polydisperse systems [33].

Although a direct comparison of results between studies is difficult due to the different anatomical definitions of deposition sites, the varying rates of flow applied and the models used, the results of previous studies and our study are qualitatively similar.

Typically, segmentation of the nasal cavity in published studies has been based on the location and specific function of each area, as well as the type of tissue in a given part of the nasal cavity. The regions into which the nasal cavity was divided in our study, similar to those in publications by Zwartz and Guilmette,

Liu et al., and Shen et al., correspond to approximate divisions based on nasal anatomy [27, 31, 33]. The nasal cavity model was divided into three sections representing the anterior, middle, and posterior segments on the lateral nasal wall, as well as the anterior and posterior segments on the septum.

The morphology of pollen comes in various diameters and shapes, which are subjected to different aerodynamic properties. The size of inhaled particles is one of the factors that significantly affects the efficiency of deposition in the nasal cavity [41]. Tree pollen grains typically range in size from 20 to 35 µm for allergenic hazel, alder, and birch trees, and from 40 to 90 µm for coniferous trees. The shapes that characterise them may suggest a greater tendency for the grains to aggregate due to the increased surface area of interaction between the particles. For a given plant species, the variability (geometric standard deviation) of pollen grain size released into the natural environment may be so small that it approaches the value considered monodisperse; however, there is convincing evidence that pollen and allergenic aerosols can agglomerate with PM particles present in the environment [2]. The tendency for the grains to aggregate may be relevant in laboratory studies, where pollen grains are released from powder placed in an FBD dispenser. The results of tree pollen aerosolisation show that the aerosol released from the FBD is not always monodisperse. However, for birch, alder, and hazel, most particles had a diameter of 20–35 µm, which corresponds to the size of individual grains. There is also a fraction of agglomerates ranging in size from 100 to 300 µm.

Ohsaki et al. demonstrated that particle shape influences deposition, showing that rod-shaped particles tend to have higher reachability into the depths of a simple respiratory model [40]. Hu et al., studying mugwort pollen deposition, determined the shape factor, i.e., the ratio of the surface area of a sphere with the same volume as the pollen grain to the actual surface area of an ellipsoidal *Artemisia* pollen, which turned out to be very close to 1. Thus, the researchers assumed that the orientation of the grains may have a minimal effect on their transport and deposition patterns, and therefore particle orientation was not taken into account [15]. Inhavong et al. used spheres with an equivalent aerodynamic diameter as a reference point when studying pollen particle deposition [17]. We made a similar assumption in our study.

Another factor influencing the deposition is the effective density of particles, which is related to differences in grain morphology. This can cause particles of similar size to have different masses due to different porosity. The inertial deposition plays the predominant role in the pollen deposition in the nasal cavity, and the Stokes number can characterise its efficiency:

$$\mathrm{Stk} = \frac{u\rho d^2}{18\mu L} \quad (1)$$

where u [m/s] denotes the velocity of the particle (assumed equal to the velocity of inhaled air), ρ [kg/m^3] - particle density, d [m] – particle effective diameter, μ – air viscosity [kg/(m s)], L – the characteristic size of the air channel. Higher values of Stk indicate stronger effects of particle inertia resulting in the deposition. Equation 1 shows that not only grain velocity (u) and diameter (d) enhance the inertial deposition, but also the grain density (ρ) has a positive effect. It means that a less porous (i.e., heavier) particle has a higher chance of inertial deposition than a more porous (lighter) particle with the same size.

Another factor that can affect the effective pollen density is the moisture content, which varies depending on weather conditions, making it difficult to control. Let us note, however, that particle size, d, has a greater influence (to the power of two in eq. 1) than velocity or density (linear relationship).

An important parameter for the actual value of the Stokes number is also the characteristic size of an air channel (L). In narrow or tortuous channels (low L), the Stokes number, and hence the inertial deposition, becomes higher, which explains why the area close to the nasal valve and other nasal regions characterised by narrowing or abrupt change in the flow direction, are highly loaded with pollen deposits.

In addition to inertial impaction, other physical phenomena influence the deposition of large aerosol particles such as pollen. These include: gravitational settling, electrostatic interactions, and direct interception [42]. However, gravitational settling plays only a marginal role due to the short residence time of pollen in the nose during airflow (even at the lowest flow rate, 5 L/min, the air passes through the nasal cavity in less than 0.3 s, which is too short for effective vertical displacement of particles). Electrostatic effects can be neglected mainly due to the wet, charge-conductive surface of the nose, which was also reproduced in our study by coating the anatomical model. Only direct interception remains an important deposition mechanism for large, non-spherical particles, such as pollen agglomerates, during their flow through narrow channels. The size (100 µm and larger) and complex shape of such agglomerates promote their direct contact with walls, even if the deposition by impaction is not effective (e.g., when they are light). Lack of impaction of such particles in the anterior parts of the nose allows them to penetrate and deposit in deeper parts of the nasal cavity due to interception. The above-mentioned physical effects should help to analyse our results.

In our experimental study, the anterior part of the nasal cavity, from the nostrils to the beginning of the turbinates, played a significant role in capturing pollen grains, with the filtering role of this area increasing with the size of the grains. A larger size led to an increase in particle deposition, mainly in the frontal sections of the nasal cavity. At the same time, smaller pollen grains also settled in the middle part, which agrees with the probability of inertial deposition as explained above (eq. 1.). This observation is also consistent with the results of many previously published studies using particles with a diameter corresponding to the size of tree pollen grains [33, 34, 36–38] which confirmed that the main mechanism of deposition in the frontal region is inertial impaction.

Hazeri et al. presented valuable information on the deposition of microparticles with a diameter of 1 to 40 µm in the nasal cavity using the CFD technique, at flow rates of 7.5 and 15 L/min, drawing attention to the dominant role of the anterior part of the nasal cavity, in particular the nasal vestibule and Kiesselbach's area, for

particles larger than 15 μm [34]. Schroeter et al. also demonstrated, based on the research conducted using the CFD technique, that particles approximately 30 μm in diameter are deposited mainly in the front part of the nasal cavity, especially in the area of the nasal valve and the upper part of the vestibule [36]. This observation was also supported by Inthavong et al., who used CFD to study the deposition of monodisperse particles with sizes of 10 and 20 μm at a breathing rate of 10 L/min, concluding that larger particles, due to their greater inertia, tend to settle predominantly in the frontal regions of the nasal cavity [38].

Shen et al. evaluated the deposition of lactose particles (10–109 μm) in a silicone replica of the nasal cavity at different flow rates (15, 35, and 55L/min) using optical coherence tomography as well as CFD technology, concluding that the anterior part of the nasal airways is the most effective site for particle capture, showing the most significant sediment thickness and particle density at all flow rates tested [33]. They observed that particle size affected penetration depth. Larger particles (approximately 100 μm) were deposited mainly in the anterior part of the nose replica; smaller particles showed more even distribution, also depositing in the middle and rear parts (however, they did not occur in the rear parts in CFD models) [33].

In the study by Hazeri et al., particles that settled in the middle part of the nasal cavity covered the middle turbinate to a greater extent than the inferior turbinate. The superior turbinate had a negligible amount of particles [34]. In our analysis with microscopic evaluation of slides of alder, birch, and hazel pollen deposited in the middle part of the lateral wall of the nasal cavity, pollen recorded on the middle part of the inferior turbinate was more numerous than in the middle of the middle turbinate. This may be because it is the anterior part of the middle turbinate that directly faces the oncoming flow, rather than the middle turbinate itself. Our results are similar to those of Shang et al., who demonstrated in a CFD model that took into account the external part of the nose and the breathing area that particles with a size of 20 μm are mainly deposited in the nasal vestibule and the inferior turbinate [37]. Our microscopic analysis of slides from selected pollen deposition sites on the nasal septum confirmed the highest accumulation in the anterior part of the septum.

As already discussed (eq. 1.), flow rate is another factor affecting the efficiency of particle deposition in the nasal cavity [41]. Flow rates of 5 L/min, 7.5 L/min, and 20 L/min (per nostril) were tested in our study, and it was generally observed that particle deposition on the lateral wall and nasal septum increased with increasing flow rate, reaching the highest values at 20 L/min. The total amount of deposited pollen increased in both the front and middle segments for birch, hazel, and alder pollen with a size of 18–34 μm, with higher airflow resulting in greater pollen deposition in the anterior segment. The highest flow rate resulted in the intensified accumulation of large pine and spruce pollen grains, sized 40–90 μm, in the anterior segments of the nasal cavity, maintaining this part as the primary site of deposition for both total and segmental pollen.

Our observations align with those published in several papers [32, 34, 39]. Hazeri et al. and Wang et al. concluded that higher flow velocities lead to greater particle deposition due to increased particle inertia [34, 43]. Schroeter et al. presented a study using CFD technology that examined the flow-deposition relationship for particles measuring 10–11μm. Higher flow velocities increased anterior deposition, while flow rates of 7.5 L/min maximised turbinate deposition [32]. Zwartz and Guilmette used a nasal replica to demonstrate that at higher flow rates, more particles are deposited in the nasal vestibule due to inertial impaction [27]. Studies conducted by Calmet et al., Schroeter et al., and Shen et al. also confirm the relationship between flow rates and particle deposition, demonstrating that higher flow rates tend to increase deposition efficiency, especially of larger particles in the anterior nasal regions [33, 36, 44]. However, Shen et al. research findings indicate that smaller particles tend to penetrate deeper into the nasal airways, resulting in more even deposition in both the front and back of the nose [33].

There are few studies on the deposition of specific plant pollen in the nasal cavity [14, 15]. In a study conducted by Hu et al. using CFD technology, the deposition of *Artemisia* pollen grains (20–22 μm in diameter) exhibited a consistent pattern, aligning with publications that show deposition hotspots moving forward with increasing respiratory rate [15]. They demonstrated that most wet Artemisia pollen grains settled in the anterior third of the nasal cavity, including the nasal vestibule and anterior part of the nasal septum, under conditions of increased respiratory flow typical of physical exertion, while dry Artemisia pollen more often penetrated further parts of the nasal cavity.

Our results contribute to the existing literature, demonstrating that in most cases, inertial deposition plays a dominant role due to pollen grain size. However, other factors, such as particle density or formation of large but light agglomerates of grains, may influence the regional distribution of pollen in the nasal cavity.

The study may have clinical implications; the results help determine which parts of the nasal cavity are more susceptible to the deposition of allergen-containing pollen grains, which has a significant impact on the optimization of prevention and local treatment. Potential risks depend on where pollen settles in the nasal cavity, due to the different types of epithelium and cleansing mechanisms present. Particles that do not pass through the nasal valve and settle on the skin-like squamous epithelium in the nasal vestibule that lacks a mucus coating can be easily mechanically removed by sneezing or blowing the nose. Allergens released from pollen grains, which reach the ciliated mucosa through the mucus layer and deposit on the vascular-rich mucosa, can trigger a cascade of allergic reactions leading to the onset of symptoms of allergic rhinitis in sensitized individuals. Such data should help study the links between regional deposition of pollen grains on the nasal surface and allergic response, e.g., during nasal provocation in pollen chambers. Knowledge of the sites where pollen grains are deposited in the nasal cavity facilitates the control of allergen exposure, including the use of pollen barrier protection measures and local treatment [45]. Knowledge of the impact of air flow intensity on pollen deposition confirms preventive recommendations for allergy sufferers to avoid outdoor physical activity during periods of intense pollen release by plants to which they are sensitized.

LIMITATIONS

The study has some limitations. The 3D model of the nasal cavity does not fully reflect the variability found in different individuals, nor does it take into account the influence of the nasal cycle and nose movements on particle deposition. The potential impact of nasal hairs on pollen filtration has been neglected. The study does not cover the potential impact of exacerbated allergy on the geometry of the nasal airways. Furthermore, only constant flow rates and a uniform initial grain velocity were considered, which in reality are subject to fluctuations. Since the size of hygroscopic particles may increase after inhalation, this may cause inaccuracies. Under natural conditions, patients with respiratory allergies may be exposed to aerosols containing not only pollen grains but also pollen fragments, which can also serve as carriers of allergens [46].

CONCLUSIONS

To our knowledge, this is the first study focusing on the experimental evaluation of regional tree pollen deposition in a 3D model of the nasal cavity at different flow rates. The original methods for such analysis were developed, including the macroscopic analysis of photographs showing the spots of deposited pollen on the surface of the anatomical model of the nasal cavity, and microscopic evaluation of pollen collected from selected parts of the nasal geometry. The macroscopic analysis was augmented by the original software for quantitative determination of the areas covered by the deposited pollen. The results showed statistically significant differences in the regional deposition of different types of pollen in the nose, depending on flow conditions.

The study confirms the role of inertial effects in aerosol flow and deposition in the nose, indicating that the large size of pollen grains and higher airflow rates promote pollen deposition mainly in the anterior regions of the lateral wall and nasal septum. However, it also shows that other deposition mechanisms, such as direct interception in the case of grain aggregates, and differences in the effective particle density, may influence the spatial distribution of deposited pollen in the nasal cavity. The results should facilitate control of allergen exposure and the use of local treatment.

REFERENCES

1. Dahl A., Galán C., Hajkova L. et al.: The Onset, Course and Intensity of the Pollen Season. In: Allergenic Pollen A Review of the Production, Release, Distribution and Health Impacts. Eds.: M. Sofiev, K.C. Bergmann. Springer Science + Business Media, Dordrecht 2013, 29–70.
2. Tager I.B.: Health Effects of Aerosols. In: Aerosols Handbook. Measurement, Dosimetry and Heath Effect. Eds.: L.S. Ruzner, N.H. Harley. Taylor & Francis. Boca Raton 2013, 565–636.
3. Skjøth C.A., Šikoparija B., Jäger S., EAN-Network.: Pollen sources. In: Allergenic Pollen A Review of the Production, Release, Distribution and Health Impacts. Eds.: M. Sofiev, K.C. Bergmann. Springer Science + Business Media, Dordrecht 2013, 9–28.
4. Puc M., Kasprzyk I.: The patterns of Corylus and Alnus pollen seasons and pollination periods in two Polish cities located in different climatic regions. Aerobiologia., 2013; 29(4): 495–511.
5. Kubik-Komar A., Piotrowska-Weryszko K., Weryszko-Chmielewska E. et al.: A study on the spatial and temporal variability in airborne Betula pollen concentration in five cities in Poland using multivariate analyses. Sci Total Environ., 2019; 660: 1070–1078.
6. Rapiejko A., Jurkiewicz D., Lipiec A.: Very high concentrations of birch pollen in the air of selected Polish cities in 2022 – clinical implication. Otolaryngol Pol., 2022; 76(6): 30–36.
7. de Weger L.A., Beerthuizen T., Gast-Strookman J.M. et al.: Difference in symptom severity between early and late grass pollen season in patients with seasonal allergic rhinitis. Clin Transl Allergy., 2011; 1: 18.
8. Caillaud D.M., Martin S., Segala C. et al: Nonlinear short-term effects of airborne Poaceae levels on hay fever symptoms. J Allergy Clin Immunol., 2012; 130(3): 812–814.
9. Behrendt H., Becker W.M.: Localization, release and bioavailability of pollen allergens: The influence of environmental factors. Current Opinion in Immunolog., 2001; 13: 709–715.
10. Raith M., Swoboda I.: Birch pollen. The unpleasant herald of spring. Front Allergy., 2023; 4: 1181675.
11. Moitra S., Kavitha B.: Aerobiology for clinicians. In: Textbook of Diagnostic and Therapeutic Procedures in Allergy. Eds.: P.K. Vedanthan, H.S. Nelson, H.P. van Bever, M.R. Murali. Taylor & Francis Group. USA 2024, 361–373.
12. Gilles S., Mariani V., Bryce M. et al.: Pollen allergens do not come alone: pollen associated lipid mediators (PALMS) shift the human immune system towards a T(H2-dominated response). J Allergy Clin Immunol., 2009; 5: 3–9.
13. Johnsen S.G.: Computational Rhinology: Unraveling discrepancies between in silico and in vivo nasal airflow assessments for enhanced clinical decision support. Bioengineering., 2024; 11: 239–321.
14. Zhang Y., Zhang L.Y., Huang F. et al.: Computational investigation of Artemisia pollen deposition in realistic nasal cavities of residents in northwest China. Zhonghua Er Bi Yan Hou Tou Jing Wai Ke Za Zhi., 2019; 54(10): 741–747.
15. Hu Z., Ma R., Wang Y.: Quantitative study of Artemisia pollens deposition in the upper airways of children with adenoidal hypertrophy. J Aerosol Science., 2023; 172: 106191.
16. Ma R., Hu Z., Tian L. et al.: Numerical and experimental analysis of pollen inhalation exposure in nasal airways following various middle turbinectomy. Sci Total Environ., 2024; 907: 168156.
17. Inthavong K., Shang Y., Del Gaudio J.M. et al.: Inhalation and deposition of spherical and pollen particles after middle turbinate resection in a human nasal cavity. Respir Physiol Neurobiol., 2021; 294: 103769.
18. Zhang Y., Ma R., Wang Y. et al.: Effect of nasal swell body on nasal airflow and Artemisia pollen deposition. Lin Chuang Er Bi Yan Hou Tou Jing Wai Ke Za Zhi., 2023; 37(7): 535–541.
19. Galán C., Smith M., Thibaudon M. et al.: Pollen monitoring: Minimum Requirements and Reproducibility of Analysis. Aerobiologia., 2014; 30: 385–395.
20. Galan C., Artaitti A., Bonnini M. et al.: Recommended terminology for aerobiological studies. Aerobiologia., 2017; 33: 293–295.
21. Stawoska I., Myszkowska D., Oliwa J. et al.: Air pollution in the places of Betula pendula growth and development changes the physicochemical properties and the main allergen content of its pollen. PLoS One., 2023; 18(1): e0279826.
22. Kormuák A., Galgóci M., Boleček P. et al.: Effect of storage on pollen viability in Pinus sylvestris L., Pinus mugo Turra and their hybrid swarms. Dendrobiology., 2019; 82: 43–51.
23. Sosnowski T.R., Rapiejko A., Sosnowski K. et al.: Development and validation of the method for experimental analysis of pollen deposition in an anatomical model of the human nasal cavity. In: Chemical and Process Engineering for Environment and Health. Current Status in 2024. Eds.: T.R. Sosnowski, M. Szwast. Łukasiewicz – Instytut Technologii Eksploatacji Wydawnictwo Naukowe, Radom 2024, 144–152.
24. Brüning J., Hildebrandt T., Heppt W. et al.: Characterization of the airflow within an average geometry of the healthy human nasal cavity. Scientific Reports., 2020; 10: 3755.

25. Rapiejko P., Sosnowski T.R., Sova J., Jurkiewicz D.: Deposition of intranasal glucocorticoids– preliminary study. Otolaryngol Pol., 2015; 69(6): 30–38.
26. Sosnowski T.R., Rapiejko P., Sova J., Dobrowolska K.: Impact of physicochemical properties of nasal spray products on drug deposition and transport in the pediatric nasal cavity model. International Journal of Pharmaceutics., 2020; 574: 118911.
27. Zwartz G.J., Guilmette R.A.: Effect of flow rate on particle deposition in a replica of a human nasal airway. Inhal Toxicol., 2001; 13(2): 109–127.
28. Oh J.W.: Pollen Allergy in a Changing World. A Guide to Scientific Understanding and Clinical Practice. 2nd ed. Springer, Singapore 2023, 41–58.
29. Agashe S.N., Caulton E.: Pollen and Spores. Applications with Special Emphasis on Aerobiology and Allergy. Science Publishers, Enfield (New Hampshire) 2009.
30. Grega L., Anderson S., Cheetham M. et al.: Aerodynamic characteristics of saccate pollen grains. Int J Plant Sci., 2013; 174: 499–510.
31. Liu Y., Matida E.A., Johnson M.R.: Experimental measurements and computational modeling of aerosol deposition in the Carleton-Civic standardized human nasal cavity. J Aerosol Sci., 2010; 41: 569–586.
32. Schroeter J.D., Tewksbury E.W., Wong B.A. et al.: Experimental measurements and computational predictions of regional particle deposition in a sectional nasal model. J Aerosol Med Pulm Drug Deliv., 2015; 28(1): 20–29.
33. Shen Z., Tolu Mekonne T.T., Cai X. et al.: Experimental measurements of particle deposition in the human nasal airway. Int J Pharm., 2025; 672: 125280.
34. Hazeri M., Faramarzi M., Sadrizadeh S. et al.: Regional deposition of the allergens and micro-aerosols in the healthy human nasal airway. Journal of Aerosol Science., 2021; 152: 105700.
35. Schroeter J.D., Garcia G.J., Kimbell J.S.: Effects of Surface Smoothness on Inertial Particle Deposition in Human Nasal Models. J Aerosol Sci., 2011; 42(1): 52–63.
36. Schroeter J., Kimbell J.S. Asgharian B.: Analysis of Particle Deposition in the Turbinate and Olfactory Regions Using a Human Nasal Computational Fluid Dynamics Model. J Aerosol Med., 2006; 19(3): 301–313.
37. Shang Y.D., Inthavong K., Tu J.Y.: Detailed micro-particle deposition patterns in the human nasal cavity influenced by the breathing zone. Comput. Fluids., 2015; 114: 141–150.
38. Inthavong K., Tian Z.F., Tu J.Y. et al.: Optimising nasal spray parameters for efficient drug delivery using computational fluid dynamics. Comput Biol Med., 2008; 38 (6): 713–726.
39. Kimbell J.S., Segal R.A., Asgharian B. et al.: Characterization of deposition from nasal spray devices using a computational fluid dynamics model of the human nasal passages. J Aerosol Med., 2007; 20 (1): 59–74.
40. Ohsaki S., Mitani R., Fujiwara S. et al.: Effect of particle-wall interaction and particle shape on particle deposition behaviour in human respiratory system. Chemical & Pharmaceutical Bulletin., 2019; 67(12): 1328–1336.
41. Guo Y., Tang Y., Su Y., Sun D.: Influencing factors of particle deposition in the human nasalcavity. Laryngoscope Investigative Otolaryngology., 2024; 9(4): e1308.
42. Cheng Y.S.: Mechanisms of pharmaceutical aerosol deposition in the respiratory tract. AAPS Pharm Sci Tech., 2014; 15: 630–640.
43. Wang S.M., Inthavong K., Wen J. et al.: Comparison of micron- and nanoparticle deposition patterns in a realistic human nasal cavity. Respir Physiol Neurobiol., 2009; 166(3): 142–151.
44. Calmet H., Kleinstreuer C., Houzeaux G. et al.: Subject-variability effects on micron particle deposition in human nasal cavities. J. Aerosol Sci., 2018; 115: 12–28.
45. Chen X., Deng C., Mi J. et al.: Barrier Protection Measures for the Management of Allergic Rhinitis: A Systematic Review and Meta-analysis. Am J Rhinol Allergy., 2020; 34(4): 564–572.
46. de Weger L.A., Bergmann K.C., Rantio-Lehtimäki A. et al.: Impact of pollen. In: Allergenic Pollen A Review of the Production, Release, Distribution and Health Impacts. Eds.: M. Sofiev, K.C. Bergmann. Springer Science + Business Media, Dordrecht 2013, 161–215.